Article

Mutations that prevent caspase cleavage of RIPK1 cause autoinflammatory disease

https://doi.org/10.1038/s41586-019-1828-5

Received: 5 March 2019

Accepted: 17 October 2019

Published online: 11 December 2019

Najoua Lalaoui[1,2,17*], Steven E. Boyden[3,17*], Hirotsugu Oda[3,17], Geryl M. Wood[3], Deborah L. Stone[3], Diep Chau[1], Lin Liu[1,2], Monique Stoffels[3], Tobias Kratina[1], Kate E. Lawlor[4,5], Kristien J. M. Zaal[6], Patrycja M. Hoffmann[3], Nima Etemadi[1,2], Kristy Shield-Artin[1,2], Christine Biben[1,2], Wanxia Li Tsai[7], Mary D. Blake[7], Hye Sun Kuehn[8], Dan Yang[9], Holly Anderton[1,2], Natasha Silke[1], Laurens Wachsmuth[10,11], Lixin Zheng[12], Natalia Sampaio Moura[3], David B. Beck[3], Gustavo Gutierrez-Cruz[13], Amanda K. Ombrello[3], Gineth P. Pinto-Patarroyo[3], Andrew J. Kueh[1,2], Marco J. Herold[1,2], Cathrine Hall[1], Hongying Wang[3], Jae Jin Chae[3], Natalia I. Dmitrieva[9], Mark McKenzie[1,2], Amanda Light[1], Beverly K. Barham[3], Anne Jones[3], Tina M. Romeo[3], Qing Zhou[3], Ivona Aksentijevich[3], James C. Mullikin[14], Andrew J. Gross[15], Anthony K. Shum[16], Edwin D. Hawkins[1,2], Seth L. Masters[1,2], Michael J. Lenardo[12], Manfred Boehm[9], Sergio D. Rosenzweig[8], Manolis Pasparakis[10,11], Anne K. Voss[1,2], Massimo Gadina[7], Daniel L. Kastner[3,18*] & John Silke[1,2,18*]

RIPK1 is a key regulator of innate immune signalling pathways. To ensure an optimal inflammatory response, RIPK1 is regulated post-translationally by well-characterized ubiquitylation and phosphorylation events, as well as by caspase-8-mediated cleavage[1–7]. The physiological relevance of this cleavage event remains unclear, although it is thought to inhibit activation of RIPK3 and necroptosis[8]. Here we show that the heterozygous missense mutations D324N, D324H and D324Y prevent caspase cleavage of RIPK1 in humans and result in an early-onset periodic fever syndrome and severe intermittent lymphadenopathy—a condition we term 'cleavage-resistant RIPK1-induced autoinflammatory syndrome'. To define the mechanism for this disease, we generated a cleavage-resistant *Ripk1*^{D325A} mutant mouse strain. Whereas *Ripk1*$^{-/-}$ mice died postnatally from systemic inflammation, *Ripk1*$^{D325A/D325A}$ mice died during embryogenesis. Embryonic lethality was completely prevented by the combined loss of *Casp8* and *Ripk3*, but not by loss of *Ripk3* or *Mlkl* alone. Loss of RIPK1 kinase activity also prevented *Ripk1*$^{D325A/D325A}$ embryonic lethality, although the mice died before weaning from multi-organ inflammation in a RIPK3-dependent manner. Consistently, *Ripk1*$^{D325A/D325A}$ and *Ripk1*$^{D325A/+}$ cells were hypersensitive to RIPK3-dependent TNF-induced apoptosis and necroptosis. Heterozygous *Ripk1*$^{D325A/+}$ mice were viable and grossly normal, but were hyper-responsive to inflammatory stimuli in vivo. Our results demonstrate the importance of caspase-mediated RIPK1 cleavage during embryonic development and show that caspase cleavage of RIPK1 not only inhibits necroptosis but also maintains inflammatory homeostasis throughout life.

Members of three families presented with a previously undescribed autoinflammatory disorder characterized by fevers and pronounced lymphadenopathy beginning in early childhood and continuing throughout adulthood (Fig. 1a) From birth or shortly thereafter, all affected individuals experienced fevers usually occurring approximately every 2–4 weeks, lasting 1–7 days, and reaching temperatures as high as 40–41 °C. Some individuals reported extreme chills, severe headaches, and/or hallucinations that coincided with their fevers. These flares were accompanied by intermittent episodes of cervical, axillary, inguinal and/or periaortic lymphadenopathy that often caused pain or discomfort (Fig. 1b, Table 1). Several individuals experienced splenomegaly and/or hepatomegaly, which were generally more prominent early in life, as well as oral ulcers, arthralgia or gastrointestinal symptoms such as abdominal pain, nausea, diarrhoea, constipation, loss of appetite or weight loss (Table 1). Patient 7 (P7) exhibited a more chronic inflammation with acute exacerbation. Study participants often had increased levels of inflammatory markers even during symptom-free periods. In contrast to some more severe autoinflammatory disorders, there were no signs of rash, arthritis, genital ulcers or end-stage organ damage and the condition was not life-threatening in any of the patients (Table 1).

Lymphocyte counts were normal between flares in the seven affected participants (Extended Data Table 1). However, pro-inflammatory cytokines were increased in the serum from P7 when inflamed but not

A list of affiliations appears at the end of the paper.

during a flare (Fig. 1c). Transcriptomic analysis from P7 whole-blood RNA revealed an enrichment of several inflammatory gene signatures (Fig. 1d, Extended Data Fig. 1a, b). Affected members of family 2 had all taken prednisone during flares, with varying degrees of acute relief but without long-term prevention of future episodes (Table 1). Participants P1, P6 and P7 had tonsillitis (Table 1), but tonsillectomy did not improve symptoms. Similarly, the IL-1 receptor antagonist, anakinra, and the TNF antagonist, etanercept, did not suppress inflammation in patients P1, P2, P4 or P7 (Table 1). However, treatment with the IL-6 receptor antagonist tocilizumab markedly, and in some cases severely, reduced the severity and frequency of the symptoms of P1, P2, P3, P6 and P7 (Fig. 1e, Table 1, Extended Data Table 2a). Tocilizumab also provided some initial relief to P4, but P4 reported aggravation of pre-existing oral ulcers, and P6 reported eventual onset of hand pain, and both participants elected to discontinue treatment (Table 1).

Identification of pathogenic mutations in *RIPK1*

Exome sequencing in P1 and her unaffected parents and all eight members of family 2 revealed that *RIPK1* was the only gene in which a variant from both families satisfied filtering criteria. A third mutation in *RIPK1* was later discovered in family 3. Affected individuals from the three families had different heterozygous missense mutations at the same crucial aspartate residue required for RIPK1 cleavage by caspase-8 (Fig. 1f). The D324N and D324Y mutations occurred de novo in families 1 (Extended Data Fig. 2) and 3, respectively, whereas D324H was inherited in an autosomal dominant pattern in family 2. These mutations are not reported in variant databases (Extended Data Table 2b), and none of the families had rare co-segregating coding or splice mutations in genes previously implicated in autoimmune lymphoproliferative syndrome (ALPS) or other monogenic autoinflammatory disorders. Mutations in the RIPK1 cleavage site were not found in an additional 554 individuals with sporadic unexplained fever, lymphadenopathy, ALPS or idiopathic Castleman disease that we screened by Sanger or targeted hybrid capture sequencing (Extended Data Table 2c). We therefore designated this condition as cleavage-resistant RIPK1-induced autoinflammatory (CRIA) syndrome.

The optimal caspase-8 cleavage motif is highly conserved in vertebrates (Fig. 1g, Extended Data Table 3). RIPK1 can be cleaved by both caspase-6 and caspase-8, yielding products of similar size, although the caspase-6 cleavage site has not been defined[9–11]. Consistent with these reports, RIPK1 mutants found in the patients—as well as the D324A mutant that has previously[6] been shown to prevent RIPK1 cleavage by caspase-8—were resistant to both caspase-6 and caspase-8 cleavage in vitro, which suggests that the cleavage sites of caspase-6 and caspase-8 are the same (Fig. 1h).

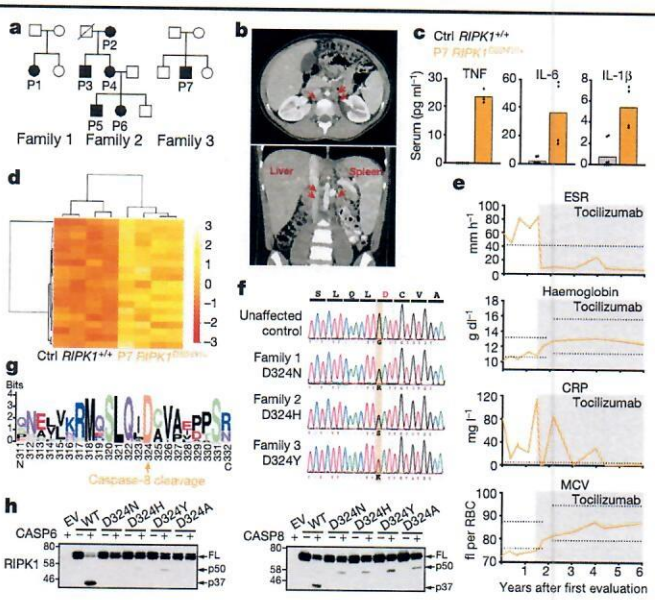

Fig. 1 | Heterozygous mutations of the RIPK1 caspase-8 cleavage site cause autoinflammatory disease. a, Affected individuals (filled symbols) in three families carried mutations in RIPK1 D324. Crossed symbol indicates a deceased individual. **b**, Axial (top) and coronal (bottom) planes of abdominal computerized tomography scans of participant P1 at age 11, after 2 months on tocilizumab but before substantial resolution of symptoms, revealing periaortic lymphadenopathy (arrows), splenomegaly (14 cm craniocaudal length), and liver at upper limit of normal (16 cm craniocaudal length). **c**, Serum cytokine levels of two P7 samples taken within 1 week, both during infliximab and before tocilizumab treatment, and four unrelated adolescent controls (ctrl). Dots are from technical duplicates for each time point. Graphs show mean. **d**, RNA sequencing of whole-blood RNA from P7 (two time points, as in **c**) and two unrelated adolescent unaffected controls, both with technical duplicates. Heat map shows differentially expressed inflammatory response genes (GO: 0006954). For gene names, see Supplementary Fig. 1. **e**, Response to tocilizumab infusion in P1. Erythrocyte sedimentation rate (ESR), C-reactive protein (CRP), haemoglobin and mean corpuscular volume (MCV) were measured serially before and after the start of tocilizumab treatment (grey shading). Time after the initial evaluation of this subject at age 10 years is depicted on the *x* axis. Horizontal lines indicate high values (ESR and CRP) or high and low values (haemoglobin and MCV) for the subject age-specific laboratory reference ranges for these markers. RBC, red blood cell count. **f**, *RIPK1* DNA sequence chromatograms show heterozygous single-base substitutions. **g**, WebLogo demonstrating conservation of the caspase-8 cleavage tetrapeptide motif in RIPK1 (human numbering) in 184 vertebrate species. **h**, In vitro caspase assays on wild-type (WT) and RIPK1 mutants. Western blots are representative of two independent experiments. For gel source data, see Supplementary Fig. 2.

Lack of RIPK1 cleavage causes embryonic lethality

To investigate the molecular mechanism for CRIA syndrome and characterize the role of RIPK1 cleavage in vivo, we generated RIPK1 cleavage-resistant mice. Rather than choosing one of the disease-associated variants, we mutated the aspartate to alanine. Although the heterozygous *Ripk1*$^{D325A/+}$ mice were viable and grossly normal, the homozygous *Ripk1*$^{D325A/D325A}$ mice died during mid-embryogenesis; much earlier than the postnatal lethality of the *Ripk1*$^{-/-}$ mice[12–15] (Fig. 2a, Extended Data Fig. 3a). *Ripk1*$^{D325A/D325A}$ lethality occurred between embryonic day 10.5 (E10.5) and E11.5, with the embryos showing several sites of mild-to-severe haemorrhage beginning in the cephalic vascular plexus, in the midbrain and hindbrain, but ultimately affecting the entire embryo including the pharyngeal arches and the pericardial space (Fig. 2a). At E11.5, all *Ripk1*$^{D325A/D325A}$ embryos were dead and displayed major haemorrhage in several locations (Fig. 2a, Extended Data Fig. 3a). E10.5 *Ripk1*$^{D325A/D325A}$ embryos had endocardial cushion hypoplasia, smaller limbs buds and a thinner neural retina (Fig. 2b). These developmental delays might be due to the defective vasculature, associated with extensive cell death observed in the yolk sac of these embryos (Fig. 2c). This phenotype was reminiscent of several strains of knockout mice with defects in TNF signalling, including *Casp8*$^{-/-}$ mice[8,16–22]. The E10.5 lethality of *Casp8*$^{-/-}$ mice is TNF-dependent[12], and can be prevented by loss of either *Ripk3* or *Mlkl*[8,22,23], which suggests that the lethality is due to TNF-induced activation of the necroptotic pathway that is normally inhibited by caspase-8. These findings led to the idea that cleavage of RIPK1 by caspase-8 inhibits necroptosis during embryogenesis[8,22]. However, *Ripk1*$^{D325A/D325A}$*Ripk3*$^{-/-}$ mice were not viable, consistent with a previous report[24]. Nevertheless, loss of RIPK3 extended survival more than loss of MLKL, which indicates that RIPK3 has a non-necroptotic role in the early embryonic lethality (Fig. 2d, Extended Data Fig. 3b). Combined loss of *Casp8* and *Ripk3* in these mice prevented the embryonic lethality, which suggests that caspase-8 does more than inhibiting RIPK1/RIPK3/MLKL-induced necroptosis

Table 1 | Clinical features of patients with CRIA syndrome

	Family 1	Family 2					Family 3
Mutation	**Asp324Asn**	**Asp324His**					**Asp324Tyr**
Patient number	**P1**	**P2**	**P3**	**P4**	**P5**	**P6**	**P7**
Gender	F	F	M	F	M	F	M
Age at evaluation (years)	10	82	55	54	22	20	13
Age at onset	2 months	Birth	2 weeks	Birth	Birth	Birth	6 months
Recurrent fevers	+	+	+	+	+	+	+
Fever maximum (°C/°F)	40.5/105	41/106	38.9/102	40.5/105	41/106	41/106	40.5/105
Fever frequency	1/2 week	1/month	1/3 weeks	1/2 weeks	1/3 weeks	1/2 weeks	1–3/2 weeks
Fever duration	3–7 days	3 days	3–5 days	2–5 days	2–5 days	3–5 days	1 day
Lymphadenopathy	+	+	+	+	+	+	+
Splenomegaly	+	–	–	–	+	+	+
Hepatomegaly	–	–	–	–	+	+	–
Tonsillitis	+	–	–	–	–	+	+
Abdominal pain	+	–	+	–	–	+	+
Rash	–	–	–	–	–	–	–
Oral ulcers	–	–	+	+	+	+	+
Genital ulcers	–	–	–	–	–	–	–
Arthritis	–	–	–	–	–	–	–
Arthralgia	–	–	+	–	–	+	+
Autoantibodies	+ ANA	+ RF	–	–	–	NA	–
Response to:							
Prednisone	+	+	+	+	+	+	+
Colchicine	NA	–	–	–	–	–	–
Anti-IL-1R	–	–	NA	–	NA	NA	–
Anti-TNF	–	–	NA	–	NA	NA	±
Anti-IL-6R	+	+	+	±D	NA	+D	+

Family 2 was first evaluated at the NIH in 1999 for unexplained periodic fever, but the data shown here are from their first return visit after identification of their *RIPK1* mutation. For fever frequency, '1/2 weeks' means once every 2 weeks.
±, partial or mixed response; ANA, antinuclear antibody; D, discontinued treatment after less than 1 year owing to reported side effects; NA, not applicable; RF, rheumatoid factor.

at this embryonic stage (Fig. 2d, Extended Data Fig. 3b). Although loss of *Ripk1* ameliorates the ALPS-like disorder observed in *Casp8*$^{-/-}$*Ripk3*$^{-/-}$mice[8,12,13,15], lack of RIPK1 cleavage did not notably affect it (Extended Data Fig. 3c, d), consistent with observations in *Fadd*$^{-/-}$*Ripk3*$^{-/-}$*Ripk1*$^{D325A/D325A}$ mice[24]. Interestingly, inhibition of RIPK1 kinase activity also rescued the embryonic lethality of *Ripk1*$^{D325A/D325A}$ (Fig. 2d). However, *Ripk1*$^{D138N,D325A/D138N,D325A}$ mice were runty and did not survive past weaning (Fig. 2d, e). These mice had a multi-organ inflammation presenting with skin hyperplasia, infiltration of leukocytes in the liver and the lung, disorganized splenic architecture and scattered cleaved caspase-3-positive cells in these organs (Extended Data Fig. 3e). Loss of one allele of *Ripk3* or *Casp8* prolonged the survival of *Ripk1*$^{D138N,D325A/D138N,D325A}$ mice to 5 weeks of age, and complete loss of *Ripk3* rescued the inflammatory phenotype of *Ripk1*$^{D138N,D325A/D138N,D325A}$ mice (Fig. 2d, e).

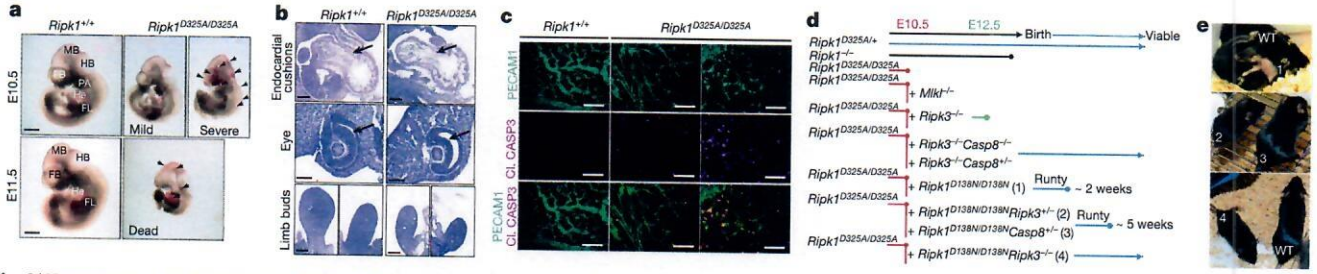

Fig. 2 | Homozygous mutation of the RIPK1 caspase-8 cleavage site in mice causes early embryonic lethality. a, E10.5 (top) and E11.5 (bottom) embryos, representative of four embryos per genotype. FB, forebrain; HB, hindbrain; He, heart; FL, forelimb; MB, midbrain; PA, pharyngeal arches. Arrows denote sites of haemorrhage. Scale bars, 900 µm (E10.5) and 1,400 µm (E11.5). **b**, Haematoxylin and eosin (H&E)-stained section of E10.5 embryos, representative of three embryos per genotype. Arrows denote endocardial cushions (top) and neural retina (middle). Scale bars, 200 µm. **c**, E10.5 yolk sacs stained with anti-PECAM1 (cyan) and anti-cleaved caspase-3 (Cl. CASP3; magenta) antibodies. Images with severely and less severely disrupted vasculature are shown. Scale bars, 50 µm. Images are representative of four embryos per genotype. **d**, Diagram depicting the extent of viability of different strains of *Ripk1*^{D325A} mice. **e**, Representative pictures of three mice per genotype numbered in **d**.

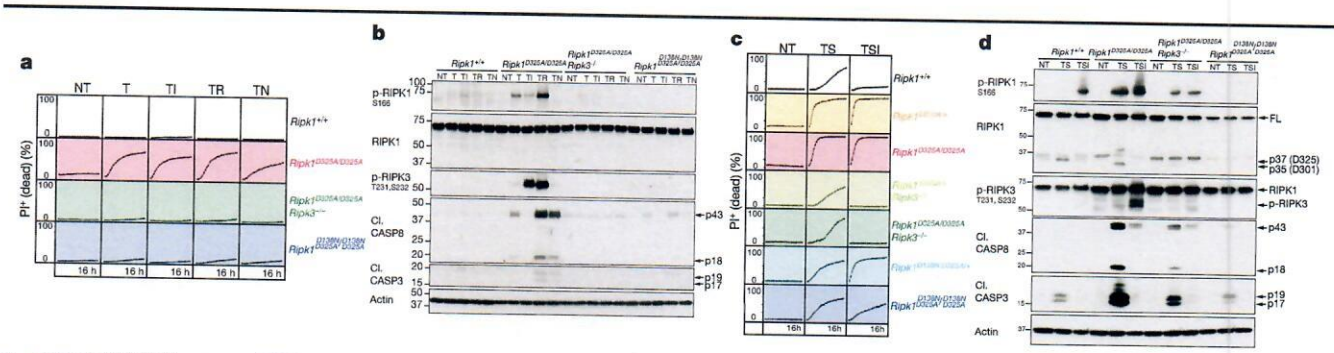

Fig. 3 | *Ripk1*$^{D325A/D325A}$ and *Ripk1*$^{D325A/+}$ cells are hypersensitive to TNF-induced death. a, **c**, Cell death of MEFs, monitored by time-lapse imaging of propidium iodide (PI) staining over 16 h. I denotes 5 μM caspase-8 inhibitor; N denotes 10 μM necrostatin; NT denotes untreated; R denotes 1 μM RIPK3 inhibitor; S denotes 100 nM SMAC mimetic; T denotes 100 ng ml^{-1} (**a**) or 10 ng ml^{-1} (**c**) TNF. Graphs are representative of four independent experiments performed with two biological repeats per genotype. **b**, **d**, Western blot of MEFs treated as in **a** for 2 h (**b**), and as in **c** for 2 h (**d**). Results are representative of two independent experiments. p-RIPK1, phosphorylated RIPK1. β-Actin was used as a loading control. For gel source data, see Supplementary Fig. 2.

RIPK1 cleavage limits TNF-induced cell death

To explore the function of RIPK1 cleavage in TNF signalling, we tested homozygous *Ripk1*$^{D325A/D325A}$ mouse embryonic fibroblasts (MEFs) for their response to TNF-induced cell death. Notably, even though TNF is not usually cytotoxic, we found that *Ripk1*$^{D325A/D325A}$ MEFs were sensitive to TNF alone and this induced increased phosphorylation of RIPK1, as well as activation of caspase-8 when compared to wild-type MEFs (Fig. 3a, b). Although inhibiting caspases or RIPK3 kinase activity did not affect cell death induced by TNF, genetic loss of RIPK3 or RIPK1 kinase activity significantly reduced TNF-induced cell death (Fig. 3a, b). Loss of RIPK3 not only completely abrogated death, but also blocked RIPK1 phosphorylation and caspase activation (Fig. 3a, b).

Given that the patients contain *RIPK1* mutations in only one allele, we tested the sensitivity of several *Ripk1*$^{D325A/+}$ heterozygous cell types to TNF. In contrast to homozygote *Ripk1*$^{D325A/D325A}$ MEFs, none of the tested *Ripk1*$^{D325A/+}$ cell types were sensitive to TNF alone (Extended Data Fig. 4a, b). However, inhibitors that directly activate the cytotoxic activity of RIPK1 (for example, SMAC mimetic, or TAK1, IKK or MK2 inhibitors)[1–4,6,25,26] rapidly sensitized *Ripk1*$^{D325A/+}$ MEFs and mouse dermal fibroblasts (MDFs) to low-dose TNF (Fig. 3c, Extended Data Fig. 4a, c). By contrast, only SMAC mimetic and TAK1 inhibitor sensitized *Ripk1*$^{D325A/+}$ bone-marrow-derived macrophages (BMDMs) to low-dose TNF (Extended Data Fig. 4b). In *Ripk1*$^{D325A/D325A}$ MEFs, TNF-induced cell death was more pronounced after the addition of IKK or TAK1 inhibitors or a combination of SMAC mimetic and MK2 inhibitor (Extended Data Fig. 4c). In addition, homozygote and heterozygote *Ripk1*^{D325A} MEFs and MDFs were slightly more sensitive to apoptosis induced by low-dose TNF and cycloheximide (Extended Data Fig. 4a, c).

Treatment with TNF plus SMAC mimetic induced a strong phosphorylation of RIPK1 and RIPK3, as well as activation of caspase-8 and caspase-3, in *Ripk1*$^{D325A/+}$ cells (Extended Data Fig. 4d–f), which was more pronounced in the *Ripk1*^{D325A} homozygote cells (Fig. 3d, Extended Data Fig. 4f). This increase in cell death induced by TNF plus SMAC mimetic correlated with increased formation of a RIPK1–caspase-8-containing complex 2 (Extended Data Fig. 4g).

Notably, given the increase in caspase-8 activation, loss of RIPK3 markedly delayed cell death induced by TNF plus SMAC mimetic or TAK1, IKK or MK2 inhibitors in both *Ripk1*^{D325A} homozygote and heterozygote fibroblasts (Fig. 3c, Extended Data Fig. 4a, c). In fibroblasts, loss of RIPK3 correlated with significantly reduced autophosphorylation of RIPK1 and caspase activation after TNF and SMAC mimetic treatment (Fig. 3d, Extended Data Fig. 4d, e). However, inhibition of RIPK3 kinase had little effect on the induction of cell death (Extended Data Fig. 4a–c), which suggests that RIPK3 contributes mostly in a structural capacity to the activation of caspase-8 in *Ripk1*^{D325A} cells.

We next analysed both *Ripk1*^{D138N,D325A} homozygote and heterozygote cells and, as expected, genetic loss of RIPK1 kinase activity prevented RIPK1 autophosphorylation (Fig. 3d, Extended Data Fig. 4d). It also provided some protection from cell death and this effect was mirrored by treatment with the RIPK1 inhibitor necrostatin (Fig. 3c, Extended Data Fig. 4a–c). Similar to RIPK3 loss, this correlated with reduced caspase-8 activation (Fig. 3d, Extended Data Fig. 4d). Together, these results indicate that in fibroblasts, RIPK3 promotes caspase-8 activation in a manner that is independent of its kinase activity and mostly independent of RIPK1 kinase activity (Fig. 3a, b), unless RIPK1 is further activated by an activating stimulus, such as SMAC mimetic (Fig. 3c, d).

One surprising observation was that the strong activation of caspase-8 in *Ripk1*^{D325A} cells led to RIPK1 cleavage (Fig. 3d, Extended Data Figs. 4d, f, 5a). In the case of the heterozygote cells, this was almost certainly due to cleavage of the wild-type protein; however, we also detected a slightly smaller RIPK1 cleavage product in homozygote cells (Fig. 3d, Extended Data Figs. 4f, 5a). This was the result of an alternative cleavage site (D301 in mouse) that is as well-conserved as the canonical site (Extended Data Fig. 5, Extended Data Table 2b). However, possibly owing to the unfavourable hydrophobic amino acid in the P1′ position[27], the D301 site was far less efficiently cleaved than the D325 site and only when the canonical site was mutated (Fig. 3d, Extended Data Figs. 4f, 5).

RIPK1 cleavage limits inflammatory responses

Patients with CRIA syndrome have recurrent fevers, so to understand how loss of RIPK1 cleavage might affect the response to inflammatory stimuli, we tested the responsiveness of the *Ripk1*$^{D325A/+}$ mice to Toll-like receptor (TLR) ligands. Although there was not a marked difference in levels of IL-6, the levels of TNF and IL-1β were higher in the *Ripk1*$^{D325A/+}$ sera after injection of a non-lethal dose of either lipopolysaccharide (LPS) or polyinosinic:polycytidylic acid (poly(I:C)) (Fig. 4a, Extended Data Fig. 6a). Similarly, PBMCs from P7 produced more TNF and IL-1β after LPS or poly(I:C) treatment (Fig. 4b, Extended Data Fig. 6b). Despite these increased levels of cytokines, hypothermia induced by LPS was not life-threatening (Extended Data Fig. 6c), which was also consistent with the symptoms of the patients with CRIA syndrome. BMDMs also produced more TNF after TLR activation (Fig. 4c), which correlated with the amount of cell death induced (Extended Data Fig. 6d).

To define the contribution of the haematopoietic compartment to the hyper-inflammatory phenotype, we generated bone marrow chimaeras. Notably, both wild-type mice transplanted with *Ripk1*$^{D325A/+}$ haematopoietic cells and *Ripk1*$^{D325A/+}$ mice transplanted with wild-type bone marrow were hyper-responsive to LPS compared with the controls (Fig. 4d). Although our data suggest that the increased inflammatory response in mice correlates with increased cell death in *Ripk1*$^{D325A/+}$

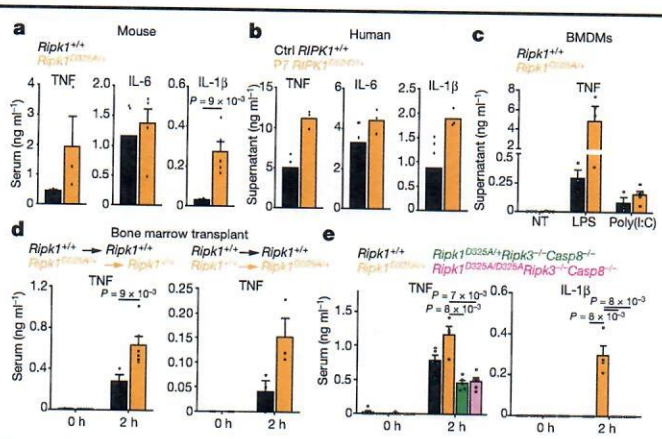

Fig. 4 | RIPK1 cleavage limits inflammation in vivo. a, Serum cytokine levels after 2 h treatment with 2 mg kg^{-1} LPS. Data are mean ± s.e.m., $n = 3$ mice for TNF and $n = 5$ mice for IL-6 and IL-1β. **b**, Cytokine levels in the supernatant of two unrelated adolescent controls (*RIPK1*$^{+/+}$) and P7 *RIPK1*$^{D324Y/+}$ PBMCs treated for 3 h with 10 ng ml^{-1} LPS. Data are mean of triplicates. **c**, TNF levels in the supernatant of BMDMs treated for 24 h with 25 ng ml^{-1} LPS or 2.5 μg ml^{-1} poly(I:C). Data are mean ± s.e.m., $n = 3$ for *Ripk1*$^{+/+}$ and $n = 3$–4 for *Ripk1*$^{D325A/+}$. **d**, Serum TNF levels in wild-type mice reconstituted with *Ripk1*$^{D325A/+}$ haematopoietic cells (left) or *Ripk1*$^{D325A/+}$ mice reconstituted with wild-type haematopoietic cells (right), treated for 2 h with 2 mg kg^{-1} LPS. Data are mean ± s.e.m., $n = 3$ and 4 *Ripk1*$^{+/+}$ → *Ripk1*$^{+/+}$, $n = 6$ *Ripk1*$^{D325A/+}$ → *Ripk1*$^{+/+}$, $n = 3$ for *Ripk1*$^{+/+}$ → *Ripk1*$^{D325A/+}$ mice per genotype. **e**, Serum cytokines levels after 2 h treatment with 2 mg kg^{-1} of LPS. Data are mean ± s.e.m., $n = 4$ for *Ripk1*$^{D325A/+}$, $n = 5$ for the other genotypes. Results in **a**, **c** and **e** are representative of two independent experiments. Each dot in **a** and **c**–**e** represents a mouse. All *P* values determined by unpaired, two-tailed *t*-test.

cells, RIPK1 also contributes to the activation of NF-κB and MAPK signalling pathways[14,28–30]. However, loss of RIPK1 cleavage did not affect TNF-induced NF-κB or MAPK activation in either mouse cells or patient-derived dermal fibroblasts (Extended Data Fig. 6e–g). Furthermore, the cytokine increases observed in the *Ripk1*$^{D325A/+}$ sera were dependent on RIPK3 and caspase-8, which suggests that cell death is the major contributor to cytokine induction in these mice (Fig. 4e).

RIPK1 has a role in activating NF-κB and MAPK inflammatory pathways, caspase-8-mediated apoptosis and RIPK3-dependent necroptosis. Each of these distinct responses can contribute to inflammatory signalling and it has been difficult to disentangle which pathway causes inflammation in any given physiological situation. We describe a human autoinflammatory disorder caused by heterozygous mutations in RIPK1 seemingly constrained to a single, evolutionarily conserved aspartate residue at the caspase-6/8 cleavage site. Mutation of this key aspartate prevents caspase-6/8 cleavage of RIPK1, sensitizes cells to TNF-induced cell death and causes embryonic lethality in homozygous mice. Several mechanisms inhibit cell death after TNF stimulation[1–7,26,31] and our data emphasize how important this is in limiting an inflammatory response. Pathogens may counter cell-death-mediated inflammation by expressing caspase-8 inhibitors and a cellular defensive mechanism that amplifies the cell death response in the absence of RIPK1 cleavage makes intuitive sense, and may explain why some pathogens also attempt to cleave RIPK1[32,33]. Previously, pathogen inhibition of caspase-8 was thought to unleash the necroptotic pathway; however, RIPK1 cleavage not only limits necroptosis, as previously assumed, but can also limit caspase-8-mediated apoptosis. Furthermore, the kinase activities of RIPK3 and RIPK1 have mainly been thought of as activators of necroptosis. However, the rescue of the postnatal lethal phenotype of the *Ripk1*^{D138N,D325A} mice by loss of *Casp8* or *Ripk3* reveals a far more complex interaction between these molecules than previously anticipated. Our data provide support for the concept of a hierarchy of preferred responses to TNF signalling: cell survival, then caspase-8-mediated apoptosis, with necroptosis as a last resort (Extended Data Fig. 7). Notably, despite the fact that most of our knowledge of RIPK1 function comes from analyses of TNF signalling, and that TNF has a pivotal role in many inflammatory diseases, patients with CRIA syndrome responded to the IL-6 inhibitor tocilizumab but did not respond to TNF inhibitors. It will be interesting therefore to determine what role RIPK1 has in IL-6-mediated inflammation.

Online content

Any methods, additional references, Nature Research reporting summaries, source data, extended data, supplementary information, acknowledgements, peer review information; details of author contributions and competing interests; and statements of data and code availability are available at https://doi.org/10.1038/s41586-019-1828-5.

1. Bertrand, M. J. M. et al. cIAP1 and cIAP2 facilitate cancer cell survival by functioning as E3 ligases that promote RIP1 ubiquitination. *Mol. Cell* **30**, 689–700 (2008).
2. Dondelinger, Y. et al. MK2 phosphorylation of RIPK1 regulates TNF-mediated cell death. *Nat. Cell Biol.* **19**, 1237–1247 (2017).
3. Dondelinger, Y. et al. NF-κB-independent role of IKKα/IKKβ in preventing RIPK1 kinase-dependent apoptotic and necroptotic cell death during TNF signaling. *Mol. Cell* **60**, 63–76 (2015).
4. Jaco, I. et al. MK2 phosphorylates RIPK1 to prevent TNF-induced cell death. *Mol. Cell* **66**, 698–710.e5 (2017).
5. Feltham, R. et al. Mind bomb regulates cell death during TNF signaling by suppressing RIPK1's cytotoxic potential. *Cell Reports* **23**, 470–484 (2018).
6. Menon, M. B. et al. p38^{MAPK}/MK2-dependent phosphorylation controls cytotoxic RIPK1 signalling in inflammation and infection. *Nat. Cell Biol.* **19**, 1248–1259 (2017).
7. Lafont, E. et al. TBK1 and IKKε prevent TNF-induced cell death by RIPK1 phosphorylation. *Nat. Cell Biol.* **20**, 1389–1399 (2018).
8. Oberst, A. et al. Catalytic activity of the caspase-8–FLIP$_L$ complex inhibits RIPK3-dependent necrosis. *Nature* **471**, 363–367 (2011).
9. Kim, J. W., Choi, E. J. & Joe, C. O. Activation of death-inducing signaling complex (DISC) by pro-apoptotic C-terminal fragment of RIP. *Oncogene* **19**, 4491–4499 (2000).
10. Lin, Y., Devin, A., Rodriguez, Y. & Liu, Z. G. Cleavage of the death domain kinase RIP by caspase-8 prompts TNF-induced apoptosis. *Genes Dev.* **13**, 2514–2526 (1999).
11. van Raam, B. J., Ehrnhoefer, D. E., Hayden, M. R. & Salvesen, G. S. Intrinsic cleavage of receptor-interacting protein kinase-1 by caspase-6. *Cell Death Differ.* **20**, 86–96 (2013).
12. Dillon, C. P. et al. RIPK1 blocks early postnatal lethality mediated by caspase-8 and RIPK3. *Cell* **157**, 1189–1202 (2014).
13. Kaiser, W. J. et al. RIP1 suppresses innate immune necrotic as well as apoptotic cell death during mammalian parturition. *Proc. Natl Acad. Sci. USA* **111**, 7753–7758 (2014).
14. Kelliher, M. A. et al. The death domain kinase RIP mediates the TNF-induced NF-κB signal. *Immunity* **8**, 297–303 (1998).
15. Rickard, J. A. et al. RIPK1 regulates RIPK3-MLKL-driven systemic inflammation and emergency hematopoiesis. *Cell* **157**, 1175–1188 (2014).
16. Moulin, M. et al. IAPs limit activation of RIP kinases by TNF receptor 1 during development. *EMBO J.* **31**, 1679–1691 (2012).
17. Peltzer, N. et al. LUBAC is essential for embryogenesis by preventing cell death and enabling haematopoiesis. *Nature* **557**, 112–117 (2018).
18. Peltzer, N. et al. HOIP deficiency causes embryonic lethality by aberrant TNFR1-mediated endothelial cell death. *Cell Reports* **9**, 153–165 (2014).
19. Varfolomeev, E. E. et al. Targeted disruption of the mouse *Caspase 8* gene ablates cell death induction by the TNF receptors, Fas/Apo1, and DR3 and is lethal prenatally. *Immunity* **9**, 267–276 (1998).
20. Yeh, W. C. et al. FADD: essential for embryo development and signaling from some, but not all, inducers of apoptosis. *Science* **279**, 1954–1958 (1998).
21. Yeh, W. C. et al. Requirement for Casper (c-FLIP) in regulation of death receptor-induced apoptosis and embryonic development. *Immunity* **12**, 633–642 (2000).
22. Kaiser, W. J. et al. RIP3 mediates the embryonic lethality of caspase-8-deficient mice. *Nature* **471**, 368–372 (2011).
23. Alvarez-Diaz, S. et al. The pseudokinase MLKL and the kinase RIPK3 have distinct roles in autoimmune disease caused by loss of death-receptor-induced apoptosis. *Immunity* **45**, 513–526 (2016).
24. Zhang, X., Dowling, J. P. & Zhang, J. RIPK1 can mediate apoptosis in addition to necroptosis during embryonic development. *Cell Death Dis.* **10**, 245 (2019).
25. Dondelinger, Y. et al. Serine 25 phosphorylation inhibits RIPK1 kinase-dependent cell death in models of infection and inflammation. *Nat. Commun.* **10**, 1729 (2019).
26. Geng, J. et al. Regulation of RIPK1 activation by TAK1-mediated phosphorylation dictates apoptosis and necroptosis. *Nat. Commun.* **8**, 359 (2017).
27. Stennicke, H. R. & Salvesen, G. S. Catalytic properties of the caspases. *Cell Death Differ.* **6**, 1054–1059 (1999).
28. Wong, W. W. et al. RIPK1 is not essential for TNFR1-induced activation of NF-κB. *Cell Death Differ.* **17**, 482–487 (2010).
29. Newton, K. et al. RIPK1 inhibits ZBP1-driven necroptosis during development. *Nature* **540**, 129–133 (2016).

30. Cuchet-Lourenço, D. et al. Biallelic *RIPK1* mutations in humans cause severe immunodeficiency, arthritis, and intestinal inflammation. *Science* **361**, 810–813 (2018).
31. Micheau, O., Lens, S., Gaide, O., Alevizopoulos, K. & Tschopp, J. NF-kappaB signals induce the expression of c-FLIP. *Mol. Cell. Biol.* **21**, 5299–5305 (2001).
32. Croft, S. N., Walker, E. J. & Ghildyal, R. Human Rhinovirus 3C protease cleaves RIPK1, concurrent with caspase 8 activation. *Sci. Rep.* **8**, 1569 (2018).
33. Pearson, J. S. et al. EspL is a bacterial cysteine protease effector that cleaves RHIM proteins to block necroptosis and inflammation. *Nat. Microbiol.* **2**, 16258 (2017).

Publisher's note Springer Nature remains neutral with regard to jurisdictional claims in published maps and institutional affiliations.

© The Author(s), under exclusive licence to Springer Nature Limited 2019

[1]The Walter and Eliza Hall Institute, Parkville, Victoria, Australia. [2]Department of Medical Biology, University of Melbourne, Parkville, Victoria, Australia. [3]Inflammatory Disease Section, National Human Genome Research Institute, National Institutes of Health, Bethesda, MD, USA. [4]Centre for Innate Immunity and Infectious Diseases, Hudson Institute of Medical Research, Clayton, Victoria, Australia. [5]Department of Molecular and Translational Science, Monash University, Clayton, Victoria, Australia. [6]Light Imaging Section, Office of Science and Technology, National Institute of Arthritis and Musculoskeletal and Skin Diseases, National Institutes of Health, Bethesda, MD, USA. [7]Translational Immunology Section, National Institute of Arthritis and Musculoskeletal and Skin Diseases, National Institutes of Health, Bethesda, MD, USA. [8]Department of Laboratory Medicine, Clinical Center, National Institutes of Health, Bethesda, MD, USA. [9]Translational Vascular Medicine Branch, National Heart, Lung, and Blood Institute, National Institutes of Health, Bethesda, MD, USA. [10]Institute for Genetics & Cologne Excellence Cluster on Cellular Stress Responses in Aging-Associated Diseases (CECAD), University of Cologne, Cologne, Germany. [11]Center for Molecular Medicine (CMMC), University of Cologne, Cologne, Germany. [12]Molecular Development of the Immune System Section, Laboratory of Immune System Biology; Clinical Genomics Program, National Institute of Allergy and Infectious Diseases, National Institutes of Health, Bethesda, MD, USA. [13]Laboratory of Muscle Stem Cells and Gene Regulation, National Institute of Arthritis and Musculoskeletal and Skin Diseases, National Institutes of Health, Bethesda, MD, USA. [14]NIH Intramural Sequencing Center, National Human Genome Research Institute, National Institutes of Health, Bethesda, MD, USA. [15]Division of Rheumatology, Department of Medicine, University of California San Francisco, San Francisco, CA, USA. [16]Division of Pulmonary and Critical Care, Department of Medicine, University of California San Francisco, San Francisco, CA, USA. [17]These authors contributed equally: Najoua Lalaoui, Steven E. Boyden, Hirotsugu Oda. [18]These authors jointly supervised this work: Daniel L. Kastner, John Silke. *e-mail: lalaoui@wehi.edu.au; steven.boyden@genetics.utah.edu; kastnerd@mail.nih.gov; silke@wehi.edu.au

Methods

Participant enrolment

Families were enrolled and evaluated in the Clinical Center at the National Institutes of Health under a protocol approved by the Institutional Review Board of the National Institute of Diabetes and Digestive and Kidney Diseases and the National Institute of Arthritis and Musculoskeletal and Skin Diseases. Human studies complied with relevant ethical regulations and all participants provided written informed consent. No statistical methods were used to predetermine sample size.

Tocilizumab treatment

P1 was 11 years old at the time of her first intravenous infusion of tocilizumab at a dose of 8 mg kg^{-1}. She initially received medication every 3 weeks but later reduced the frequency to every 4 or 5 weeks because of a busy school schedule. On the less frequent dosing, P1 had more breakthrough symptoms, mainly tender lymphadenopathy. In 2018, when the US FDA approved the use of the injectable form in children with juvenile idiopathic arthritis, P1 was switched to 162 mg by subcutaneous injection every 2 weeks and did very well on this regimen. P2, P3, P4 and P6 received regular self-administered tocilizumab by 162 mg subcutaneous injections starting at every 2 weeks—the standard dose and route of administration for adults. The dose frequency for P3 was gradually increased to every 6 days. P7 received an initial infusion of tocilizumab at 8 mg kg^{-1} before being switched to the subcutaneous injectable form (162 mg every 2 weeks) for convenience. On this regimen, P7 noted prompt resolution of fevers, abdominal pain and joint pain, and gradual normalization of laboratory testing, including CRP, ESR, haemaglobin, haematological indices and serum iron.

Exome sequencing

Exome capture (Illumina TruSeq v2 for family 1, Roche SeqCap EZ Exome+UTR for family 2, and IDT xGen Exome Research Panel for family 3) and sequencing (Illumina HiSeq 2000, 2500 and NovaSeq 6000) was performed for all available family members at the National Institutes of Health (NIH) Intramural Sequencing Center (NISC) using 2 × 101-, 2 × 126-, and 2 × 151-base-pair (bp) paired-end reads. The data were analysed as follows: alignment with Novoalign; duplicate marking with Picard; re-alignment, re-calibration, and variant calling with GATK; and annotation with Annovar. Variants were filtered to select those that were nonsynonymous or in splice sites within 6 bp of an exon, had less than 1% mutant allele frequency in variant databases, and co-segregated with the phenotype. The mutations were validated by Sanger sequencing in all family members, and to rule out non-paternity, non-maternity or other sample identity errors, genders and relatedness were confirmed by examining heterozygous call rates on the X chromosome, Y chromosome call rates and Mendelian inheritance error rates in the exome data.

In vitro cleavage assays

Unlabelled in vitro transcription and translation of 1 µg of empty pCMV6-Entry control vector (Origene), wild-type *RIPK1* cDNA cloned into pCMV6-Entry vector (Origene), p.D324N, p.D324H, p.D324Y and p.D324A mutant *RIPK1* constructs (GENEART Site-Directed Mutagenesis System, Invitrogen) was performed in a 50-µl reaction using the TnT T7 Quick Coupled Transcription/Translation System (Promega). We incubated 2 µl of this reaction with either 12 U of purified recombinant caspase-8 (Calbiochem), 12 U of purified recombinant caspase-6 (Calbiochem), or an equal volume of re-suspension buffer, in caspase reaction buffer from the Caspase-8 Fluorometric Assay Kit (Enzo Life Sciences) and 10 mM dithiothreitol (DTT) in a 40 µl final volume at 37 °C for 3 h. These reactions were blotted for RIPK1 using an antibody recognizing a RIPK1 C-terminal antibody (610459, BD Transduction Laboratories).

RNA sequencing

Total RNA was isolated from whole blood collected in PAXgene Blood RNA Tubes using PAXgene Blood RNA Kit (PreAnalytiX) as per the manufacturer's instructions. Total RNA was used for cDNA library preparation using the TruSeq Stranded mRNA Library Preparation kit for NeoPrep (Illumina). Sequencing was performed on an Illumina HiSeq 3000 System in a 1 × 50-bp single-read mode. Sequenced reads were mapped against the human reference genome (GRCh38) using hisat v.2.2.1.0[34]. Reads mapped to haemoglobin genes were removed from further analysis. Mapped reads were quantified using HTSeq[35,36]. All the count data were normalized using TCC[37] and differentially expressed genes were detected using edgeR[38]. Gene Ontology enrichment analysis was performed using DAVID[36].

Mice

All mouse studies complied with relevant ethical regulations and approved by the Walter and Eliza Hall Institute Animal Ethics Committee. The *Ripk1*^{D325A} and *Ripk1*^{D138N,D325A} mice were generated by the MAGEC laboratory (WEHI) on a C57BL/6J background. To generate *Ripk1*^{D325A} mice, 20 ng μl^{-1} of *Cas9* mRNA, 10 ng μl^{-1} of sgRNA (ATTTGACCTGCTCGGAGGTA) and 40 ng μl^{-1} of the oligo donor (tgtcttctcattacagAAAGAGTATCCAGATCAAAGCCCAGTGCTGCAGAG AATGTTTTCACTGCAGCATGCCTGTGTACCATTACCTCCGAGCAGGTC AAATTCAGgtaactcacctattcgttcatttgcatactcgctca) (in which uppercase bases denote exons; lowercase bases denote intron sequences) were injected into the cytoplasm of fertilized one-cell stage embryos generated from wild-type C57BL/6J breeders. To generate *Ripk1*^{D138N,D325A} mice, 20 ng μl^{-1} of *Cas9* mRNA, 10 ng μl^{-1} of sgRNA (TGACAAAGGTGTGATACACA) and 40 ng μl^{-1} of oligo donor (GGATAATCGTGGAGGCCATAGAAGGCATGTGCTACTTACAT GACAAAGGTGTGATACACAAGAACCTGAAGCCTGAGAATATCCTCGTT GATCGTGACTTTCACATTAAGgtaatccacaatctg) were injected into the cytoplasm of fertilized one-cell stage embryos generated from *Ripk1*$^{D325A/D325A}$*Ripk3*$^{-/-}$*Casp8*$^{-/+}$ breeders. Twenty-four hours later, two-cell stage embryos were transferred into the uteri of pseudo-pregnant female mice. Viable offspring were genotyped by next-generation sequencing. Targeted animals were backcrossed twice to wild-type C57BL/6J to eliminate off-target mutations and to re-integrate *Ripk3* and *Casp8* genes into *Ripk1*^{D138N,D325A} mice. The *Ripk3*$^{-/-}$ mice[39], *Casp8*$^{-/-}$ mice[19] and *Mlkl*$^{-/-}$ mice[40] were all previously described. The *Ripk3*$^{-/-}$ mice were backcrossed to C57BL/6J mice for more than ten generations.

TLR challenge

Eight-to-twelve-week-old male mice received intraperitoneal injection of either 2 mg kg^{-1} LPS or 50 µg poly(I:C). Calculations to determine group sizes were not performed, mice were not randomized but were grouped according to genotype, and experiments were blinded.

Cells

MEFs were isolated from E10.5 embryos and MDFs were isolated from mouse tails. After SV40 transformation, MEFs and MDFs were tested for mycoplasma. 293T cells (ATCC) used to produce SV40 viruses and in Extended Data Fig. 5b were tested for mycoplasma but not authenticated.

Time-lapse imaging

Percentage cell death was assayed every 30–45 min by time-lapse imaging using the IncuCyte live cell analysis imaging (Essenbioscience) or the Opera Phenix High Content Screening System (PerkinElmer) for 16 h with 5% CO_2 and 37 °C climate control. For the IncuCyte and Opera Phenix imaging, dead cells were identified by propidium iodide (0.25 µg ml^{-1}) staining, and for the Opera Phenix imaging, all cells were stained with 250nM of SiR-DNA (Spirochrome). Dyes were added to the cells 2 h before imaging and compounds were added 10 min before the start

of imaging. For the Opera Phenix imaging, images were analysed using the server-based Columbus 2.8.0 software (PerkinElmer) to identify nuclei based on SiR-DNA staining and dead cells using propidium iodide staining. Results were exported as counts per well to be processed and graphed using R Studio (https://www.R-project.org/) with the tidyverse package (https://CRAN.R-project.org/package=tidyverse).

Human and mouse cytokines measurement

Human serum and PBMC supernatant cytokine content was measured by enzyme-linked immunosorbent assay (ELISA) (R&D: SLB50, STA00C and S6050) according to the manufacturer's instructions. The measurements were performed in technical duplicates. Student's *t*-test was performed for the statistical analysis. Mouse serum and BMDMs supernatant cytokine content was measured by ELISA (eBioscience for TNF and IL-6 and R&D for IL-1β) according to the manufacturer's instructions.

Human PBMC ex vivo stimulation

Ficoll-isolated human PBMCs were serum-starved for 20 min and stimulated for 3 h with LPS (Invivogen, tlrl-3pelps) or 6 h with poly(I:C) (Invivogen, tlrl-pic). Cytokines were measured by ELISA as described above.

Reagents

The SMAC mimetic compound A, the caspase inhibitor IDN-6556 (Idun Pharmaceuticals) and the RIPK1 inhibitor necrostatin were synthesized by TetraLogic Pharmaceuticals. The RIPK3 inhibitor GSK'872 was from Calbiochem. The TAK1 inhibitor (5Z)-7-oxozeaenol, the IKK inhibitor IKK-16 and the MK2 inhibitor PF-3644022 were from Tocris Bioscience. Cycloheximide was from Sigma. Recombinant Fc-TNF was produced in house. Ultrapure LPS-EB and poly(I:C) were purchased from Invivogen.

Immunostaining

Embryonic yolk sacs were fixed for 20 min at room temperature in 4% paraformaldehyde, blocked and permeabilized in PBS with 2% normal donkey serum (Jackson ImmunoResearch, 017-000-121) and 0.6% Triton X, probed with primary antibodies, cleaved caspase-3 (9661, CST) and PECAM1 (AF3628, R&D Systems) at 4 °C overnight, then secondary antibodies goat anti-rabbit AF488 (Invitrogen A-11008) and donkey anti-goat cy3 (705-165-147, Jackson ImmunoResearch) at room temperature for 1 h. Samples were cleared in a glycerol gradient (5–80%) overnight, whole-mounted in 80% glycerol and imaged using a DP72 microscope and cellSens Standard software (Olympus).

Immunoprecipitation

Ten million cells were seeded in 10-cm dishes. After the indicated treatments, cells were lysed in DISC lysis buffer (150 mM sodium chloride, 2 mM EDTA, 1% Triton X-100, 10% glycerol, 20 mM Tris, pH 7.5). Proteins were immunoprecipitated with 20 µl of protein G Sepharose plus 1.5 µg of FADD antibody (clone 7A2, in house) with rotation overnight at 4 °C. Beads were washed four times in DISC and samples eluted by boiling in 60 µl 1× SDS loading dye.

Western blotting

Cells lysates were separated on 4–12% gradient SDS–polyacrylamide gels (Biorad), transferred to polyvinylidene fluoride (Millipore) membranes and blotted with indicated antibodies purchased from CST except for phospho-RIPK3 (a gift from Genentech), actin (Sigma) and FADD (clone 7A2, in house). In vitro cleavage assays were blotted with a with an anti-RIPK1 antibody recognizing the C-terminal part (BD Transduction Laboratories, 610459). Cell lysates were blotted with an anti-RIPK1 antibody recognizing the N-terminal part (3493, Cell Signaling Technology).

NF-κB assay in patient-derived cells

NF-κB activation was assessed by measuring nuclear translocation of subunit p65 in fibroblasts derived from a single skin biopsy. Cells were grown overnight in 96-well plates seeded at 16,000 cells per well, and treated for 30 min with TNF (PeproTech) in PBS containing 1 mM $CaCl_2$ and 1 mM $MgCl_2$ (PBS-CM). Cells were pre-fixed for 5 min with 2% paraformaldehyde (PFA) in PBS-CM, then fixed for 10 min with 6% PFA in PBS-CM, and aldehyde groups were quenched with 50 mM NH_4Cl in PBS-CM for 15 min. After permeabilization with 0.3% SDS in PBS-CM for 5 min, cells were incubated with donkey serum dilution buffer (DSDB; 16% donkey serum, 0.3% Triton X-100, and 0.3 M NaCl in PBS) for 30 min, followed by overnight incubation at 4 °C with rabbit monoclonal NF-κB subunit p65 antibody (8242, Cell Signaling Technology) diluted at 1:500 in DSDB. Samples were then washed 3 times with permeabilization buffer (0.3% Triton X-100 and 0.1% BSA in PBS) and incubated with a 1:300 dilution of donkey anti-rabbit secondary antibody coupled to Alexa 488 (A21206, Molecular Probes) in DSDB for 1 h. Nuclei were counter-stained with a 1:2,000 dilution of SYTO 59 (Thermo Fisher) for 15 min. Automated field selection and plate imaging were performed with an IncuCyte Zoom incubator-microscopy system (Essen Bioscience) using a 20× objective. Nine fields per well of four wells per participant were pooled for analysis of nuclear p65 signal intensity. Nuclei were marked in red over a phase-contrast image, and p65 immunofluorescence was labelled in green. Overlaying a p65 mask on a nuclear mask showed both positive and negative nuclei, whereas a yellow co-staining mask showed positive nuclei only.

Reporting summary

Further information on research design is available in the Nature Research Reporting Summary linked to this paper.

Data availability

The original RNA sequencing data are uploaded and available at the Gene Expression Omnibus (GEO) under accession GSE127572. All other data are available from the corresponding authors upon reasonable request.

34. Kim, D., Langmead, B. & Salzberg, S. L. HISAT: a fast spliced aligner with low memory requirements. *Nat. Methods* **12**, 357–360 (2015).
35. Anders, S., Pyl, P. T. & Huber, W. HTSeq—a Python framework to work with high-throughput sequencing data. *Bioinformatics* **31**, 166–169 (2015).
36. Huang, W., Sherman, B. T. & Lempicki, R. A. Systematic and integrative analysis of large gene lists using DAVID bioinformatics resources. *Nat. Protocols* **4**, 44–57 (2009).
37. Sun, J., Nishiyama, T., Shimizu, K. & Kadota, K. TCC: an R package for comparing tag count data with robust normalization strategies. *BMC Bioinformatics* **14**, 219 (2013).
38. Robinson, M. D., McCarthy, D. J. & Smyth, G. K. edgeR: a Bioconductor package for differential expression analysis of digital gene expression data. *Bioinformatics* **26**, 139–140 (2010).
39. Newton, K., Sun, X. & Dixit, V. M. Kinase RIP3 is dispensable for normal NF-κBs, signaling by the B-cell and T-cell receptors, tumor necrosis factor receptor 1, and Toll-like receptors 2 and 4. *Mol. Cell. Biol.* **24**, 1464–1469 (2004).
40. Murphy, J. M. et al. The pseudokinase MLKL mediates necroptosis via a molecular switch mechanism. *Immunity* **39**, 443–453 (2013).
41. Conos, S. A., Lawlor, K. E., Vaux, D. L., Vince, J. E. & Lindqvist, L. M. Cell death is not essential for caspase-1-mediated interleukin-1β activation and secretion. *Cell Death Differ.* **23**, 1827–1838 (2016).
42. Mandal, P. et al. RIP3 induces apoptosis independent of pronecrotic kinase activity. *Mol. Cell* **56**, 481–495 (2014).
43. Newton, K. et al. Activity of protein kinase RIPK3 determines whether cells die by necroptosis or apoptosis. *Science* **343**, 1357–1360 (2014).

Acknowledgements This study was funded by the Intramural Research Programs of the National Human Genome Research Institute, the Intramural Research Program of NIH, NIH Clinical Center, National Institute of Arthritis and Musculoskeletal and Skin Diseases, National Institute of Allergy and Infectious Diseases, and National Heart, Lung, and Blood Institute, by European Research Council Advanced Grant 787826, by NHMRC grants 1025594, 1046984, 1145788, 1162765 and 1163581, NHMRC fellowships 1081421 and 1107149, by the Stafford Fox Foundation and was made possible through Victorian State Government Operational Infrastructure Support, Australian Government NHMRC IRIISS (9000433) and Australian Cancer Research Fund. N.L. is supported by project grant 1145588 from the Cancer Australia and Cure Cancer Australia Foundation and a Victorian Cancer Agency Mid-career Fellowship 17030. This work used the sequencing resources at the NIH Intramural Sequencing Center and the computational resources of the Biowulf Linux cluster at NIH (http://biowulf.nih.gov). We thank the families for their participation, D. Follmann for statistical advice, T. Uldrick and D. Fajgenbaum for assistance procuring samples, and D. Adams, A. Negro, A. Walts and Y. Yang

for clinical and technical assistance, C. Liegeois for IT assistance and the staff of the WEHI Bioservices facility for mouse husbandry. The generation of *Ripk1*^{D325A} and *Ripk1*^{D138N,D325A} mice used in this study was supported by the Australian Phenomics Network (APN) and the Australian Government through the National Collaborative Research Infrastructure Strategy (NCRIS) program.

Author contributions N.L., S.E.B. and H.O. designed and performed experiments and interpreted data. G.M.W., D.C., L.L., M.S., T.K., K.E.L., K.J.M.Z., N.E., K.S.-A., C.B., W.L.T., M.D.B., H.S.K., D.Y., H.A., N.S., L.W., L.Z., N.S.M., D.B.B., G.G.-C., C.H., H.W., J.J.C., N.I.D, M.M., A.L., Q.Z., I.A., J.C.M., A.K.V. and J.S. performed experiments. A.J.K., M.J.H., L.W. and M.P. generated the CRISPR mice. D.L.S., P.M.H., A.K.O., G.P.P.-P., B.K.B., A.J., T.M.R., A.J.G. and A.K.S. provided the clinical data. E.D.H., S.L.M., M.J.L., M.B., S.D.R. and M.G. contributed reagents, analysis and interpretation. N.L., S.E.B., D.L.K. and J.S. conceived the project and wrote the paper with input from all authors.

Competing interests The authors declare no competing interests.

Additional information

Supplementary information is available for this paper at https://doi.org/10.1038/s41586-019-1828-5.

Correspondence and requests for materials should be addressed to N.L., S.E.B., D.L.K. or J.S.

Reprints and permissions information is available at http://www.nature.com/reprints.

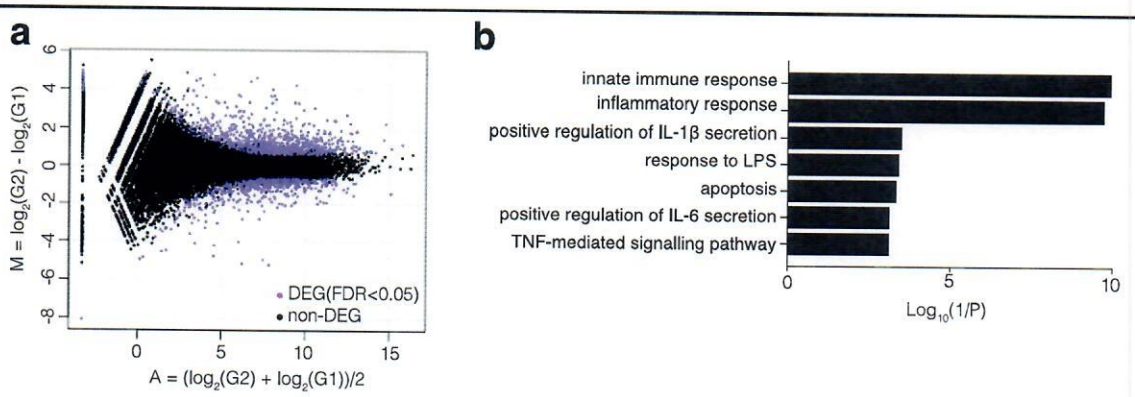

Extended Data Fig. 1 | Inflammatory gene signature in P7 whole-blood RNA. **a**, MA plot between two P7 samples and two unrelated adolescent healthy controls, both sequenced with technical duplicates. TCC-edgeR package of R followed by adjustment for multiple comparisons detected 1,394 differentially expressed genes (false discovery rate < 0.05), with 903 genes upregulated in P7, and 491 genes downregulated in P7. **b**, Representative Gene Ontology terms associated with immune signalling.

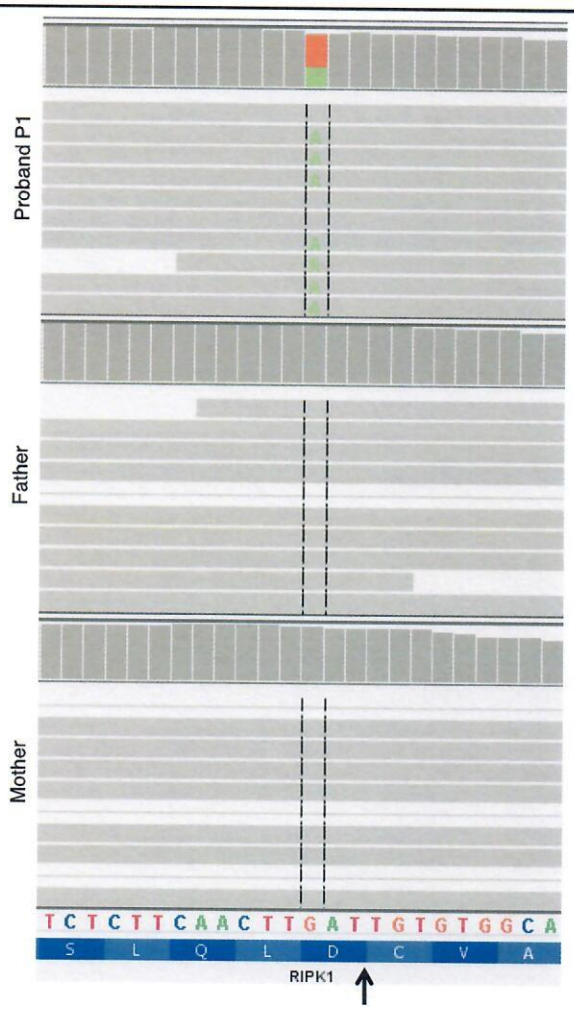

Extended Data Fig. 2 | Exome reads in family 1. Excerpts of coverage histograms and aligned exome sequence reads for the proband and her parents in family 1, displayed using the integrative genomics viewer, demonstrate de novo occurrence of the c.970G>A (p.D324N) missense mutation in the LXXD caspase-6/8 cleavage motif preceding the cleavage site (arrow). Paternity and maternity were confirmed using Mendelian inheritance error rates from the same exome data.

a

Stage		+/+	D325A/+	D325A/D325A
Weaned	Expected	45/180	90/180	45/180
	Observed	73/180	108/180	0/180
E14.5	Expected	3/12	6/12	3/12
	Observed	2/12	5/12	5/12
	Resorbed	**0/12**	**0/12**	**5/12**
E11.5	Expected	2/8	4/8	2/8
	Observed	1/8	5/8	2/8
	Dead	**0/8**	**0/5**	**2/8**
E10.5	Expected	11/44	22/44	11/44
	Observed	12/44	22/44	10/44
	Abnormal	**1/44**	**1/44**	**9/44**

b

Stage		*Ripk1*$^{D325A/D325A}$ *Ripk3*$^{-/-}$	*Mlkl*$^{-/-}$	*Casp8*$^{-/+}$	*Casp8*$^{-/-}$	*Ripk3*$^{-/-}$*Casp8*$^{-/-}$	*Ripk3*$^{-/-}$*Casp8*$^{-/+}$
Weaned	Expected	12/50	4/35	6/47	2/32	13/52	4/37
	Observed	0/50	0/35	0/47	0/32	13/52	5/37
E12.5	Expected	2/9	-	-	-	-	-
	Observed	2/9	-	-	-	-	-
	Abnormal	**1/9**	-	-	-	-	-
E11.5	Expected	-	2/10	-	-	-	-
	Observed	-	2/10	-	-	-	-
	Dead	-	**2/10**	-	-	-	-
E10.5	Expected	3/15	3/15	-	5/21	-	-
	Observed	2/15	1/15	-	1/21	-	-
	Abnormal	**0/15**	**1/15**	-	**1/21**	-	-

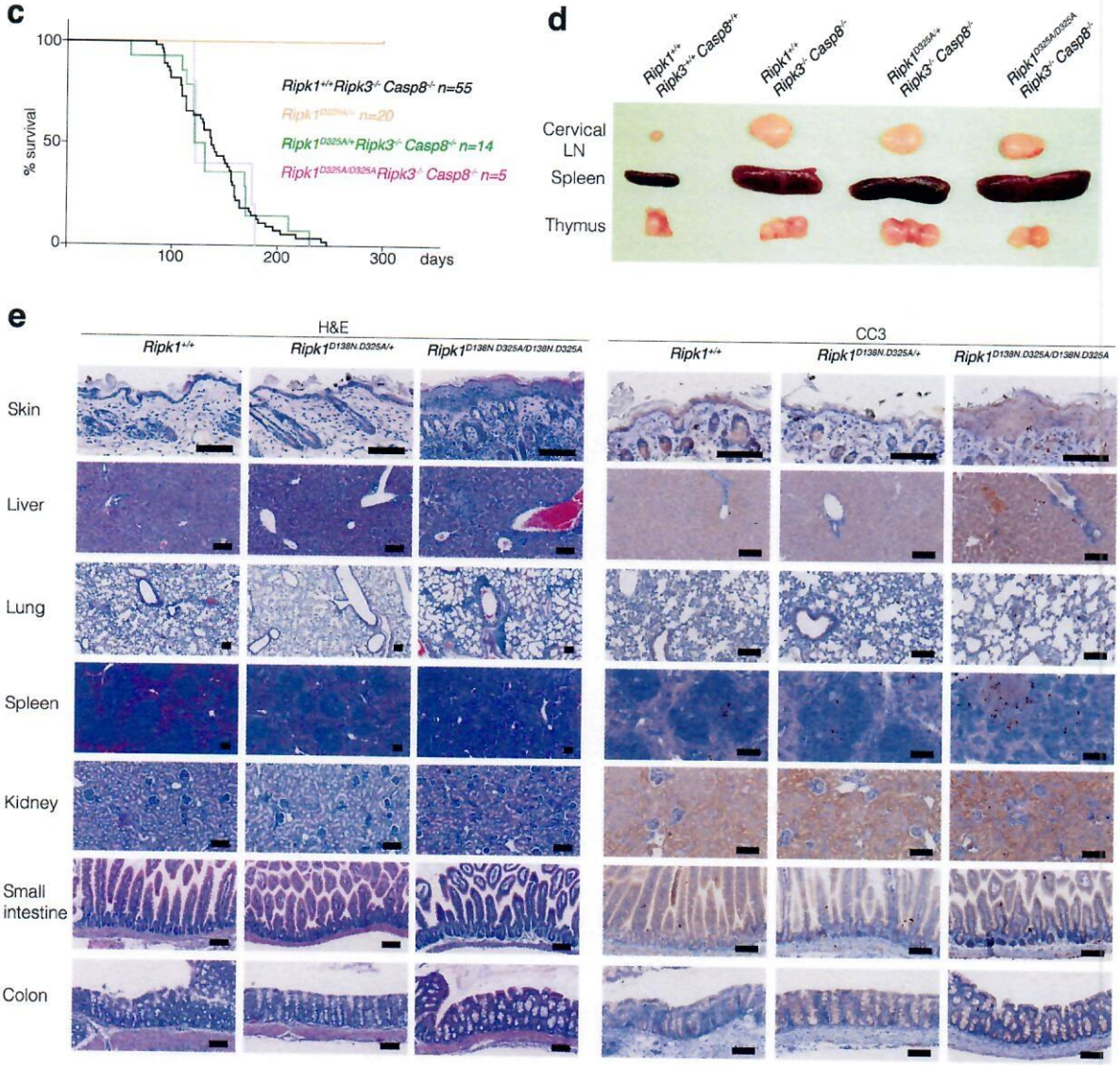

Extended Data Fig. 3 | 'Kinase-dead' RIPK1 or combined loss of *Ripk3* and *Casp8* rescue *Ripk1*$^{D325A/D325A}$ lethality. a, **b**, Observed numbers of offspring from *Ripk1*$^{D325A/+}$ intercrosses and numbers expected from Mendelian ratios at the indicated stage of development. *Ripk1*$^{D325A/D325A}$ mice are E10.5. All observed E11.5 *Ripk1*$^{D325A/D325A}$ embryos were dead and most of the E10.5 *Ripk1*$^{D325A/D325A}$ embryos were abnormal, as described in Fig. 2a, b. Loss of *Ripk3* rescued to E12.5; however, 50% of the embryos were abnormal. None of the *Ripk1*$^{D325A/D325A}$*Ripk3*$^{-/-}$ mice were born. All observed E11.5 *Ripk1*$^{D325A/D325A}$*Mlkl*$^{-/-}$ embryos were dead, showing that loss of *Mlkl* did not provide any protection. All *Ripk1*$^{D325A/D325A}$*Ripk3*$^{-/-}$*Casp8*$^{-/-}$ mice were born and developed ALPS owing to loss of *Casp8*. **c**, Kaplan–Meyer survival curves of the indicated genotypes. **d**, Cervical lymph nodes (LN), spleen and thymus of 17-week-old mice of the indicated genotypes. Pictures are representative of five mice per genotype. **e**, Tissue sections of 18-day-old *Ripk1*$^{D138N,D325A/+}$, *Ripk1*$^{D138N,D325A/D138N,D325A}$ and control mice stained with H&E (left) and anti-CC3 (brown; right). Pictures are representative of two mice per genotype.

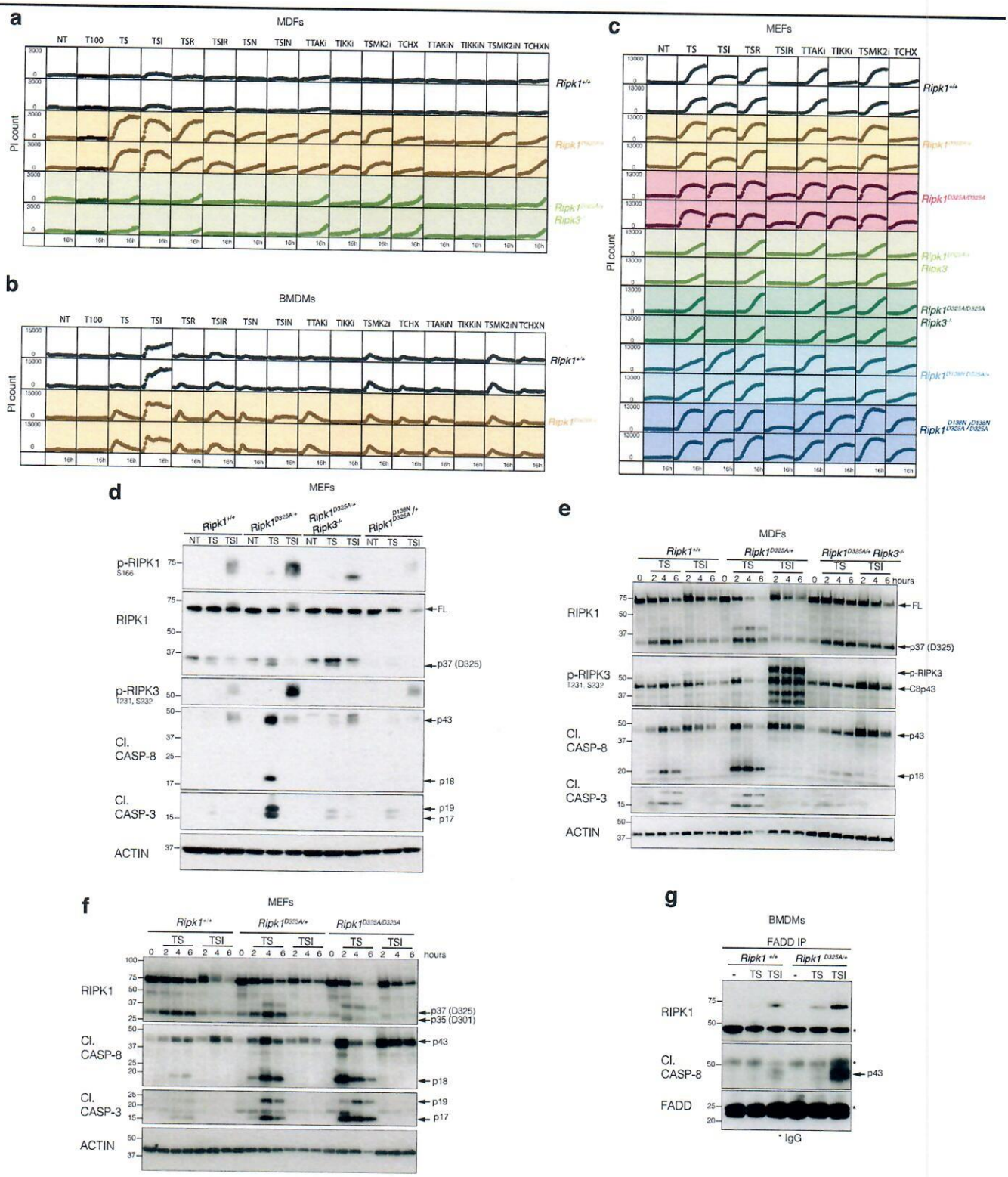

Extended Data Fig. 4 | *Ripk1*$^{D325A/+}$ cells are hypersensitive to TNF-induced death. a–c, MDFs (**a**), BMDMs (**b**) and MEFs (**c**) of the indicated genotypes were treated with either a high dose of TNF (T100; 100 ng ml^{-1}) or a low dose of TNF (T; 10 ng ml^{-1}) combined with SMAC mimetic (S; 100 nM), caspase inhibitor (I; 5 μM), RIPK3 inhibitor (R; 1 μM), necrostatin (N; 10 μM), TAK1 inhibitor (TAKi; 100 nM), IKK inhibitor (IKKi; 100 nM), MK2 inhibitor (MK2i; 2 μM) or cycloheximide (1 μg ml^{-1}) for 16 h. Cell death was quantified by propidium iodide uptake and time-lapse imaging every 30–45 min using IncuCyte. Duplicates are shown for each genotype. Graphs are representative of three (MEFs and MDFs) and two (BMDMs) biologically independent cell lines per genotype repeated independently. **d**, MEFs were treated as in Fig. 3d for 2 h. **e**, **f**, MDFs (**e**) and MEFs (**f**) were treated as in Fig. 3d for the indicated times. Results in **d**–**f** are representative of two independent experiments. β-Actin was used as a loading control. **g**, BMDMs were treated with TNF (100 ng ml^{-1}) combined with SMAC mimetic (500 nM) with or without caspase inhibitor (5 μM) for 90 min, and lysates were immunoprecipitated with anti-FADD. Results are representative of two independent experiments. For gel source data, see Supplementary Fig. 2.

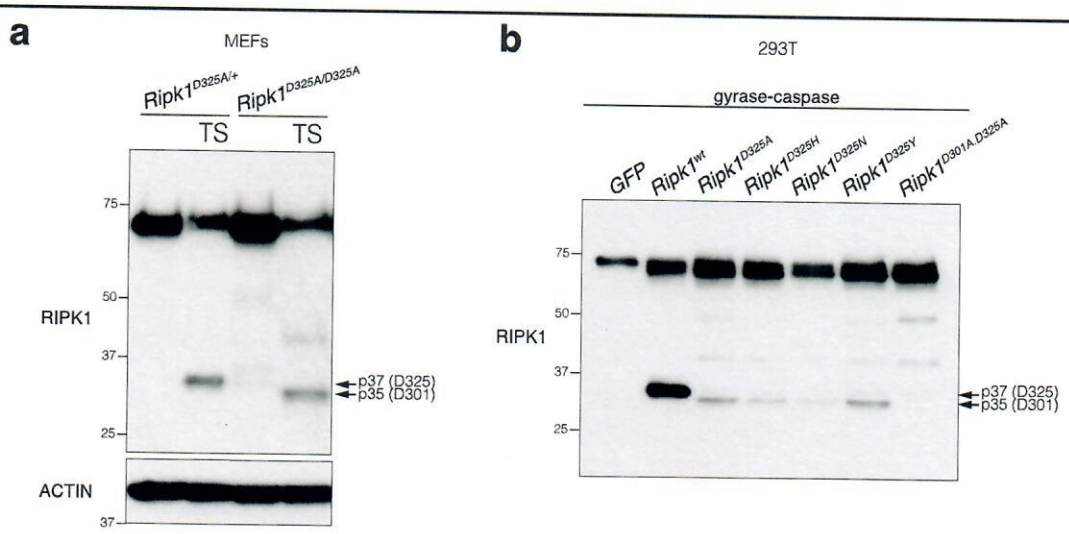

Extended Data Fig. 5 | Alternative cleavage of RIPK1. a, MEFs were treated with 10 ng ml^{-1} TNF combined with 500 nM SMAC mimetic for 2 h. **b**, Doxycycline-inducible caspase-8-gyrase[41], wild-type and mutant mouse RIPK1 constructs or GFP were co-expressed in 293T cells. Cells were treated for 2 h with 1 μg ml^{-1} doxycycline to induce caspase-8-gyrase expression and then for 2 h with 700 nM coumermycin to dimerize caspase-8-gyrase. Antibody recognizing the N-terminal end of RIPK1 was used. Results are representative of four (**a**) and two (**b**) independent experiments. For gel source data, see Supplementary Fig. 2.

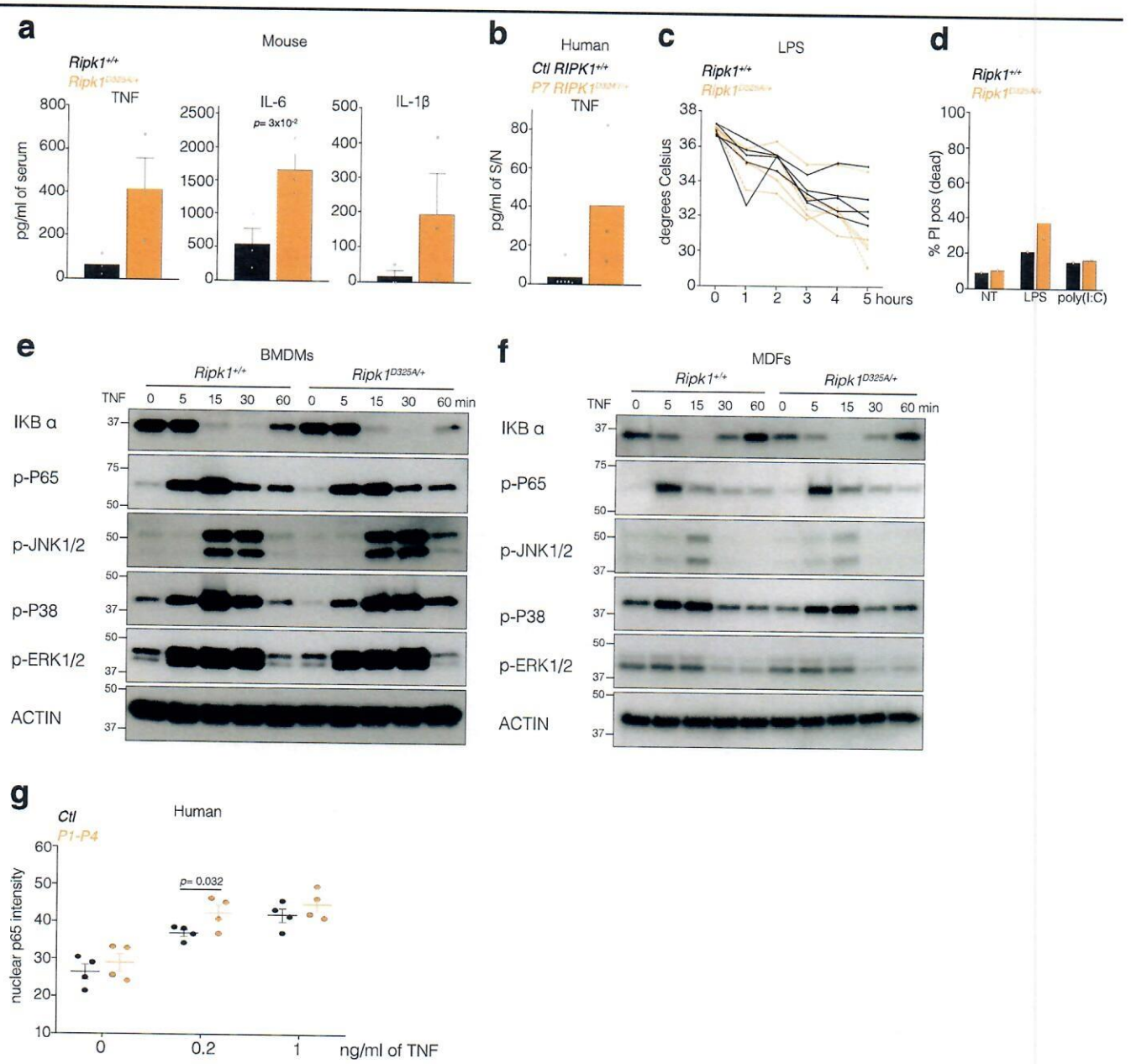

Extended Data Fig. 6 | RIPK1 cleavage limits inflammation in an NF-κB-independent manner. a, Serum cytokine levels in wild-type and *Ripk1*$^{D325A/+}$ mice treated for 3 h with 50 μg of poly(I:C). Each dot represents a mouse. Data are mean ± s.e.m., $n = 3$ mice. **b**, TNF levels in the supernatant (S/N) of two unrelated adolescent controls (Ctl *RIPK1*$^{+/+}$) and P7 *RIPK1*$^{D324Y/+}$ PBMCs treated for 3 h with 5 μg ml^{-1} poly(I:C). Data are mean of triplicates. **c**, Body temperature of mice of the indicated genotypes after injection of 2 mg kg^{-1} LPS. Each line represent a mouse; $n = 5$ mice per genotype. **d**, BMDMs of the indicated genotypes were treated for 24 h with 25 ng ml^{-1} LPS or with 2.5 μg ml^{-1} poly(I:C). Cell death was quantified by propidium iodide staining and flow cytometry. Each dot represents a biological repeat. Graph shows mean; $n = 1$ for *Ripk1*$^{+/+}$ and $n = 2$ for *Ripk1*$^{D325A/+}$. **e**, **f**, BMDMs (**e**) and MDFs (**f**) were treated with 100 ng ml^{-1} of TNF for the indicated times. Results are representative of two independent experiments. β-Actin was used as a loading control. For gel source data, see Supplementary Fig. 2. **g**, NF-κB activation in fibroblasts derived from patient skin biopsies was assessed by measuring nuclear translocation of subunit p65. Each dot represents the median of more than 1,000 single-cell measurements of nuclear mean p65 fluorescent intensities for one individual subject. Data are mean ± s.d., $n = 4$ patients and 4 controls. *P* values determined by unpaired one-tailed (**a**) or unpaired two-tailed (**g**) *t*-tests.

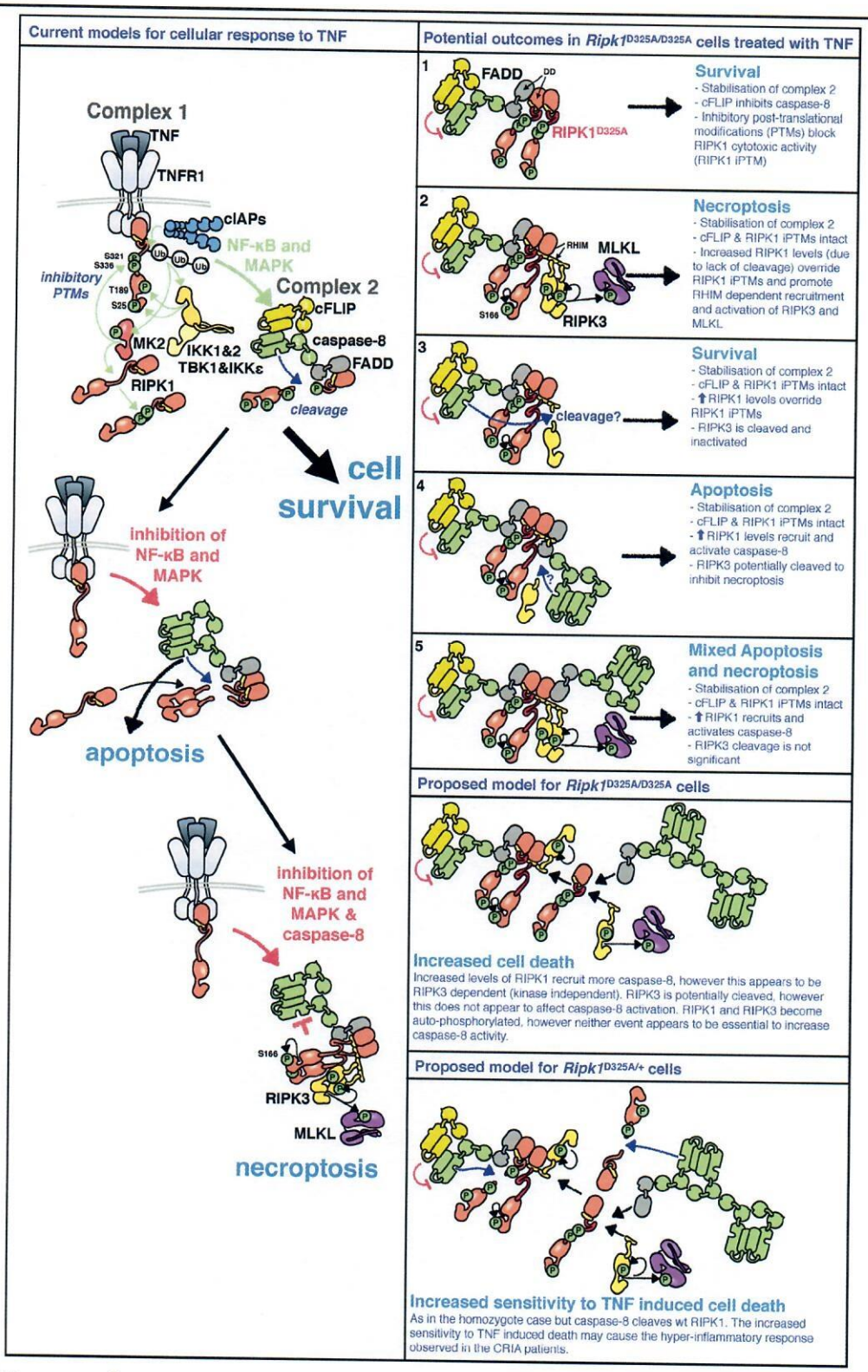

Extended Data Fig. 7 | See next page for caption.

Extended Data Fig. 7 | Proposed model for RIPK1(D325A)-induced cell death. Left, TNF binding to TNFR1 triggers the formation of complex I, and subsequent ubiquitylation and phosphorylation of RIPK1. These post-translational modifications (PTMs) inhibit the cytotoxic activity of RIPK1. Complex I formation activates NF-κB- and MAPK-dependent survival genes such as *CFLAR*, which encodes cFLIP. Subsequently, a cytosolic complex II containing FADD, caspase-8, RIPK1 and cFLIP is formed. In this complex, cFLIP inhibits caspase-8 activity so that a restricted number of substrates (such as RIPK1) are cleaved, but others (such as pro-caspase-3) are not. Cleavage of RIPK1 dismantles complex II. Activation of the NF-κB and MAPK signalling pathways PTM of RIPK1 prevent TNF from inducing cell death, resulting in cell survival (top left). Inhibition of the NF-κB or MAPK signalling pathways reduces levels of cFLIP and accelerates formation of complex II, resulting in cell death via apoptosis (middle left). When NF-κB or MAPK signalling is disrupted in caspase-8-deficient conditions, RIPK1 is not cleaved and autophosphorylates, which triggers the recruitment of RIPK3 and its autophosphorylation. RIPK3 phosphorylates MLKL and necroptosis occurs (bottom left). Right, according to this model, lack of RIPK1 cleavage could result in several distinct outcomes, as follows. (1) RIPK1 accumulation could stabilize complex II, and the presence of cFLIP and inhibitory PTMs to RIPK1 may prevent caspase-8 from killing, resulting in cell survival. (2) The accumulation of 'uncleavable' RIPK1 to complex II could override the inhibitory RIPK1 PTMs, resulting in autophosphorylation of RIPK1 and recruitment of RIPK3, leading to necroptosis. (3) RIPK1 accumulation could result in activated caspase-8 that cleaves RIPK3, resulting in cell survival. (4) Stabilization of complex II could result in recruitment and activation of caspase-8 that induces apoptosis and possibly prevents necroptosis by cleaving RIPK3. (5) Finally, the accumulation of RIPK1 could result in activation of both RIPK3 and caspase-8 and therefore induce both apoptotic and necroptotic cell death. In terms of how these potential outcomes match with our data, in homozygote *Ripk1*^{D325A} cells, both caspase-8 and RIPK3 are activated after TNF signalling, which suggests that apoptosis and necroptosis occur at the same time (Figs. 2d, 3a, b). However, according to these models, loss of RIPK3 limits caspase-8 activation (Fig. 3a, b). This suggests that the recruitment of RIPK3 to complex II increases the recruitment and activation of caspase-8. A precedent for this observation comes from experiments in which RIPK3 inhibitors promoted RIPK1-dependent caspase-8 activation[42,43], in a manner we term 'reverse activation'. In our experiments, however, RIPK3 activation occurs downstream of TNF signalling, which suggests that reverse activation might represent a physiological amplification loop that increases caspase-8 activation. Yet, this requirement for RIPK3 is not present in all cells, as the embryonic lethality of the RIPK1-cleavage mutant is only partially rescued by loss of *Ripk3*. In the heterozygote *Ripk1*^{D325A} cells, caspase-8 cleaves wild-type RIPK1, thus limiting TNF-induced cell death as compared to homozygote cells. However, reduction of cFLIP and/or RIPK1 PTMs by treatment with IAP, TAK1, IKK or translational inhibitors decreases the threshold of TNF sensitivity (Extended Data Fig. 4). This may cause the hyper-inflammatory response observed in patients with CRIA syndrome (Fig. 1).

Extended Data Table 1 | Leukocyte surface markers in patients with CRIA syndrome

			Controls		Affected subjects					
			Family 2		Family 2					Family 3
			P4 spouse	P4 son	P2	P3	P4	P5	P6	P7
		Gender	M	M	F	M	F	M	F	M
		Age at evaluation	57	22	82	55	54	22	20	12
	Percentage of leukocytes	**range**								
	Neutrophils	[34.0-67.9]	53.1	49.7	54.3	56.2	74.2^	61.9	71.5^	61.9
	Monocytes	[5.3-12.2]	9	4.5*	10.3	8.1	6.8	7.9	10.8	11.6
	Eosinophils	[0.8-7.0]	3.1	4	4.5	4.5	2.2	4	2.3	2.7
	Basophils	[0.2-1.2]	0.4	0.5	1.2	1	0.8	0.6	0.3	0.06
	Immature granulocytes	[0.0-0.4]	0.4	NA	0.4	0.3	0.3	0.7^	0.9^	0.3
	Total lymphocytes	[21.8-53.1]	34	41.2	29.3	29.9	15.7*	24.9	14.2*	22.9
Percentage of lymphocytes	**Surface markers**									
Total T	CD3+	[60.0-83.7]	79.5	81.3	83.3	62.6	82.3	83.9^	67	70
Total helper T	CD3+CD4+	[31.9-62.2]	44.6	34.5	24.2*	36.3	48.7	31.2*	30*	34.9
Helper T, naïve	CD3+CD4+CD62L+CD45RA+	[7.6-37.7]	18	22.4	2.4*	2.2*	10.2	6.7*	7.5*	18.1
Helper T, central memory	CD3+CD4+CD62L+CD45RA-	[10.4-30.7]	18.8	9.2*	17	25.1	28.4	17.6	16.7	13.2
Helper T, effector memory	CD3+CD4+CD62L-CD45RA-	[2.3-15.6]	7.1	2.8	4.8	9	7.4	6.9	5.8	3.5
Helper T, TEMRA	CD3+CD4+CD62L-CD45RA+	[0.0-1.5]	0.7	0.1	0	0	2.6^	0	0.1	3^
Total cytotoxic T	CD3+CD8+	[11.2-34.8]	32	37.5^	56.9^	20	30.2	37.9^	31.8	25.9
Cytotoxic T, naïve	CD3+CD8+CD62L+CD45RA+	[5.7-19.7]	14	26.6^	8.3	4.7*	8.5	14.2	11.4	15.8
Cytotoxic T, central memory	CD3+CD8+CD62L+CD45RA-	[1.5-10.3]	4.2	2.9	17.2^	7.9	4.6	13.8^	2.8	3.8
Cytotoxic T, effector memory	CD3+CD8+CD62L-CD45RA-	[1.1-9.2]	2.4	3.1	8.6	5.9	3.6	8.1	4.1	3.3
Cytotoxic T, TEMRA	CD3+CD8+CD62L-CD45RA+	[0.7-7.8]	11.4^	5	22.8^	1.5	13.4^	1.7	13.6^	3
Total double negative T	CD3+CD4-CD8-	[1.3-9.2]	1.6	9.2	1.8	5.5	2.1	13.9^	5	8.8
Double negative T, αβ	CD3+CD4-CD8-	[0.3-1.3]	0.3	1.4^	0.3	0.7	0.6	2.3^	1	NA
Double negative T, γδ	CD3+CD4-CD8-	[0.3-7.6]	0.9	7	0.8	4.1	1.1	10.7^	3.3	NA
Total B	CD20+	[3.0-19.0]	6.6	12.1	1.8*	10.8	11.4	3.3	12.6	12.9
Total B	CD19+	[3.3-19.3]	6.6	12.1	1.8*	10.8	11.4	3.3	12.6	12.9
Total NK	CD16+ or CD56+CD3-	[6.2-34.6]	13.6	7	15.3	26.3	6.6	13	20	17.1
Total NKT	CD16+ or CD56+CD3+	[2.2-12.4]	9.3	9	14.6^	5.8	8.4	26.7^	3.6	9.8

Percentages before tocilizumab treatment are shown. Values above or below reference ranges are marked by carets (^) or asterisks (*), respectively.
NA, not applicable; TEMRA, T effector memory re-expressing CD45RA.

Extended Data Table 2 | Effect of tocilizumab treatment and *RIPK1* caspase cleavage site mutations is absent in known autoinflammatory diseases

a

Affected subject	Months on tocilizumab	ESR (mm/hr) [0-42]	CRP (mg/L) [0-4.99]
P2	0	50	30.4
P2	12	7	0.6
P3	0	8	3.9
P3	10	2	<0.15
P3	10	1	<0.15
P3	34	2	<0.15

b

dbSNP v151
141,456 exomes and genomes from the Genome Aggregation Database (v2.1)
77,238 exomes and genomes from the Kaviar database (September 2015 release)
60,706 exomes from the Exome Aggregation Consortium (v0.3.1)
32,488 exomes from the Haplotype Reference Consortium
6,503 exomes from the NHLBI Exome Sequencing Project
2,577 genomes from the 1000 Genomes Project (August 2015 release)
662 exomes from the NHGRI ClinSeq project
95 exomes from the NIEHS Environmental Genome Project
69 genomes sequenced at Complete Genomics, Inc.

c

Phenotype	Number of subjects	RIPK1 cleavage site mutations
Unexplained recurrent fever	168	0
Lymphadenopathy	332	0
ALPS or ALPS-like	52	0
Idiopathic Castleman disease	2	0

a, Inflammatory markers in subjects treated with tocilizumab. The first time point for each subject is from 3 days before the first tocilizumab injection. P3 had two measurements from the same week at his 10-month post-tocilizumab evaluation. Reference ranges are given in brackets. **b**, Variant databases in which mutations in the *RIPK1* caspase cleavage site are absent. Variant databases are not independent.

c, Result of additional screening for mutations in the *RIPK1* caspase cleavage site.

ALPS, autoimmune lymphoproliferative syndrome; NHGRI, National Human Genome Research Institute; NHLBI, National Heart, Lung, and Blood Institute; NIEHS, National Institute of Environmental Health Sciences.

Article

Extended Data Table 3 | Conservation of RIPK1 caspase-8 cleavage site

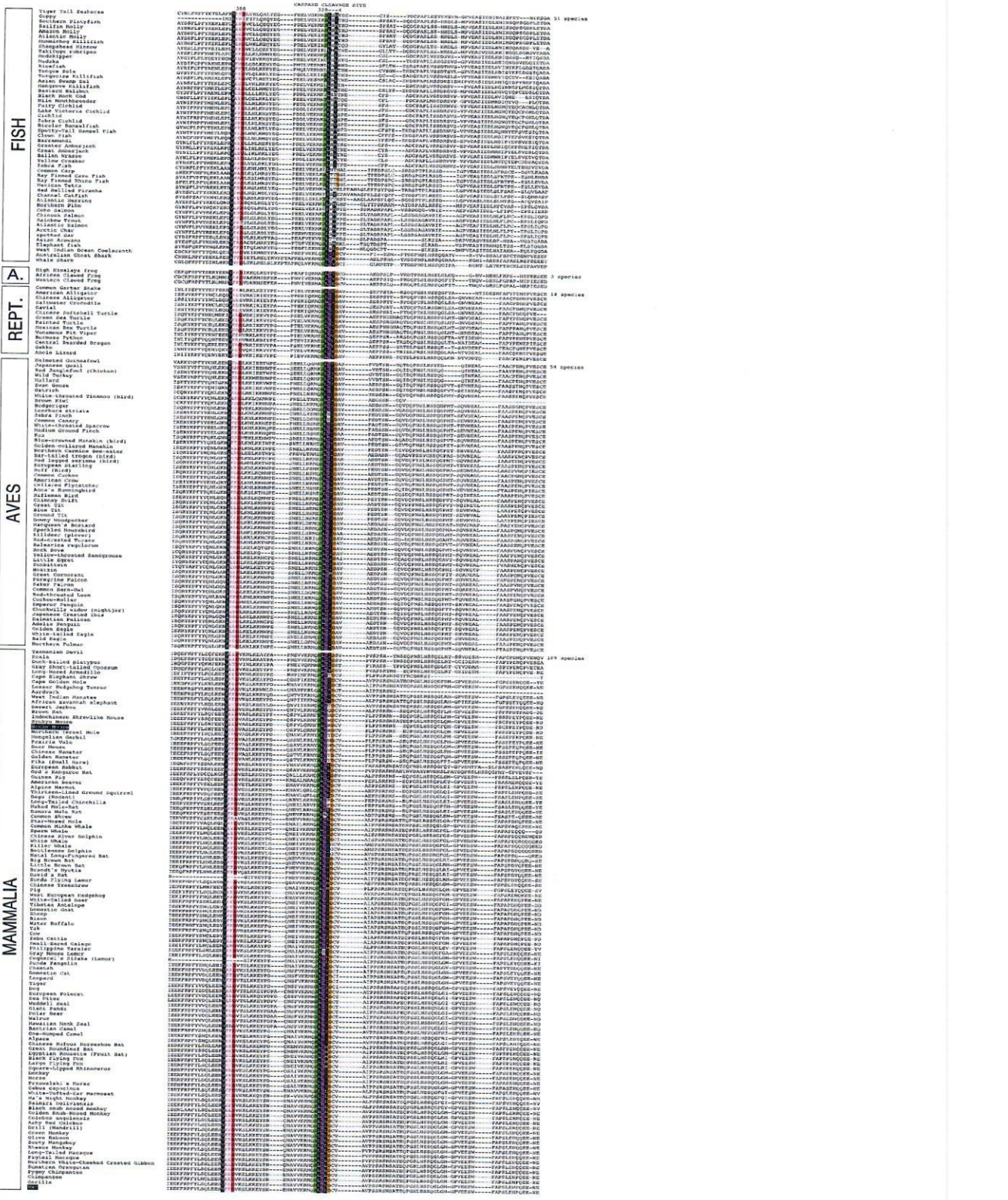

Protein sequences orthologous to human RIPK1 were aligned in 235 vertebrate species, using Multiz alignment in the UCSC Genome Browser. These include representative species from the major classes: 51 fish, 3 amphibians (A.), 14 reptiles (Rept.), 58 birds (Aves) and 109 mammals (Mammalia). Most species within these classes, except fish (7 out of 51), contain the very highly conserved D324 (human numbering) caspase cleavage site within this region. Notably, nearly all species (223) have a potential caspase cleavage site, D300; however, it is noteworthy that this Asp is in most cases succeeded by a large hydrophobic amino acid that is less favourable for caspase cleavage.

nature research

Corresponding author(s): Najoua Lalaoui

Last updated by author(s): Sep 22, 2019

Reporting Summary

Nature Research wishes to improve the reproducibility of the work that we publish. This form provides structure for consistency and transparency in reporting. For further information on Nature Research policies, see Authors & Referees and the Editorial Policy Checklist.

Statistics

For all statistical analyses, confirm that the following items are present in the figure legend, table legend, main text, or Methods section.

n/a	Confirmed	
☐	☒	The exact sample size (*n*) for each experimental group/condition, given as a discrete number and unit of measurement
☐	☒	A statement on whether measurements were taken from distinct samples or whether the same sample was measured repeatedly
☐	☒	The statistical test(s) used AND whether they are one- or two-sided *Only common tests should be described solely by name; describe more complex techniques in the Methods section.*
☒	☐	A description of all covariates tested
☒	☐	A description of any assumptions or corrections, such as tests of normality and adjustment for multiple comparisons
☐	☒	A full description of the statistical parameters including central tendency (e.g. means) or other basic estimates (e.g. regression coefficient) AND variation (e.g. standard deviation) or associated estimates of uncertainty (e.g. confidence intervals)
☒	☐	For null hypothesis testing, the test statistic (e.g. *F*, *t*, *r*) with confidence intervals, effect sizes, degrees of freedom and *P* value noted *Give P values as exact values whenever suitable.*
☒	☐	For Bayesian analysis, information on the choice of priors and Markov chain Monte Carlo settings
☒	☐	For hierarchical and complex designs, identification of the appropriate level for tests and full reporting of outcomes
☒	☐	Estimates of effect sizes (e.g. Cohen's *d*, Pearson's *r*), indicating how they were calculated

Our web collection on statistics for biologists contains articles on many of the points above.

Software and code

Policy information about availability of computer code

Data collection	Exome Sequencing was performed on an Illumina HiSeq 2000, 2500 and NovaSeq 6000). RNA Sequencing was performed on an Illumina HiSeq 3000 System. Cell death was monitored by time-lapse imaging using the IncuCyte® live cell analysis imaging (Essenbioscience) and the Opera PhenixTM High Content Screening System (PerkinElmer, USA).
Data analysis	Exome Sequencing was analyzed as follows: alignment with Novoalign; duplicate marking with Picard; re-alignment, re-calibration, and variant calling with GATK; and annotation with Annovar. RNA Sequenced reads were mapped against the human reference genome (GRCh38) using hisat v2.2.1.035. Reads mapped to hemoglobin genes were removed from further analysis. Mapped reads were quantified using HTSeq36,37. All the count data were normalized using TCC38 and differentially expressed genes were detected using edgeR39. Gene ontology enrichment analysis was performed using DAVID37. The original RNA sequencing data is uploaded and available online (Gene Expression Omnibus: GSE127572). For the Opera PhenixTM, images were analysed using the server based Columbus 2.8.0 software (PerkinElmer, USA) to identify nuclei based on SiR-DNA staining and dead cells using PI staining. Results were exported as counts per well to be processed and graphed using R Studio (https://www.R-project.org/) with the tidyverse package (https://CRAN.R-project.org/package=tidyverse).

For manuscripts utilizing custom algorithms or software that are central to the research but not yet described in published literature, software must be made available to editors/reviewers. We strongly encourage code deposition in a community repository (e.g. GitHub). See the Nature Research guidelines for submitting code & software for further information.

Data

Policy information about availability of data

All manuscripts must include a data availability statement. This statement should provide the following information, where applicable:

- Accession codes, unique identifiers, or web links for publicly available datasets
- A list of figures that have associated raw data
- A description of any restrictions on data availability

The original RNA sequencing data is uploaded and available online (Gene Expression Omnibus: GSE127572).

Field-specific reporting

Please select the one below that is the best fit for your research. If you are not sure, read the appropriate sections before making your selection.

☒ Life sciences ☐ Behavioural & social sciences ☐ Ecological, evolutionary & environmental sciences

For a reference copy of the document with all sections, see nature.com/documents/nr-reporting-summary-flat.pdf

Life sciences study design

All studies must disclose on these points even when the disclosure is negative.

Sample size	No sample size calculations were performed. For the in vitro experiments the variability between biological repeats was very low, when possible at least 3 independent biological cell lines were analysed at least twice. For in vivo experiments, for each experiments at least 3 to 5 animals per genotype were used and experiments were performed twice to ensure reproducibility.
Data exclusions	No data were excluded from the study.
Replication	Experiments were reproduced at least twice and all attempts at replication were successful.
Randomization	Mice were grouped according to genotype and animals were age- and sex-matched.
Blinding	Animal technicians were blinded to treatment conditions and temparture and body temperature measurements without any input from the experimental investigator.

Reporting for specific materials, systems and methods

We require information from authors about some types of materials, experimental systems and methods used in many studies. Here, indicate whether each material, system or method listed is relevant to your study. If you are not sure if a list item applies to your research, read the appropriate section before selecting a response.

Materials & experimental systems

n/a	Involved in the study
☐	☒ Antibodies
☐	☒ Eukaryotic cell lines
☒	☐ Palaeontology
☐	☒ Animals and other organisms
☐	☒ Human research participants
☒	☐ Clinical data

Methods

n/a	Involved in the study
☒	☐ ChIP-seq
☒	☐ Flow cytometry
☒	☐ MRI-based neuroimaging

Antibodies

Antibodies used

RIPK1 N-terminal antibody (clone D94C12, cat number 3493, Cell Signaling Technology)
RIPK1 C-terminal antibody (cat number 610459, BD Transduction Laboratories)
Phospho-RIPK1 (clone D1L3S, cat number 65746, Cell Signaling Technology)
Phospho -RIPK3 (Gift from Genetech)
Caspase-6 (clone EPR4405, cat number ab108335, Abcam)
Caspase-8 (clone E7, cat number ab32397, Abcam)
Cleaved caspase-3 (cat number 9661, Cell Signaling Technology)
Cleaved caspase-8 (clone D5B2, cat number 8592, Cell Signaling Technology)
PECAM1 (cat number AF3628, R&D Systems)
goat anti-rabbit AF488 (cat number A-11008, Invitrogen)
donkey anti-goat cy3 (cat number 705-165-147, Jackson ImmunoResearch)
FADD (clone 7A2, WEHI in house)

	IκBα (cat number 9242, Cell Signaling Technology) phospho-p65 (clone 93H1, cat number 3033, Cell Signaling Technology) p65 (clone D14E12, cat number 8242, Cell Signaling Technology) phospho-JNK1/2 (clone cat number 4668P, Cell Signaling Technology) phospho-p38 (clone D3F9, cat number 4511, Cell Signaling Technology) phospho ERK1/2 (cat number 9101 Cell Signaling Technology) β-actin (clone AC-15, cat number A-1978; Sigma-Aldrich)
Validation	Validation data for commercial antibodies are available on vendor websites. Validation of p-RIPK3 has been done on RIPK3 knock-out cells (Figure 3e). GEN135-35-9 anti-mouse phospho-RIPK3 T231, S232 is validated for WB and IHC in Newton et al (2016) Nature 540:129-133. Validation of anti FADD was with FADD knock-out cells in O'Reilly et al (2004) Cell Death Differ 11:724–736

Eukaryotic cell lines

Policy information about cell lines

Cell line source(s)	293T were from ATCC. All mouse cell line were generated from the different mice in this study.
Authentication	Mouse cell lines were sequenced to confirm the RIPK1 D325A genotyping. 293T were not authenticated.
Mycoplasma contamination	293T and most of mouse cell lines were tested and negative for mycoplasma
Commonly misidentified lines (See ICLAC register)	No commonly misidentified line was used

Animals and other organisms

Policy information about studies involving animals; ARRIVE guidelines recommended for reporting animal research

Laboratory animals	All mice are Mus musculus maintained on a C57BL/6 background. Litter-mates males of 8-12 weeks old were used for Fig 4a,e and Extended Data Fig6a. Litter-mates females of 8-12 weeks old were used for Fig 4d. Mice of both sexes of 8-12 weeks old were used for timed matings and to generate MDFs and BMDMs. Litter-mates mice of both sexes were monitor for enlarged lymph nodes and spleen until ethical point (extended data fig3c, d). Litter-mates mice of both sexes of 2 weeks old were used for HE and caspase-3 staining in Extended Data fig3e
Wild animals	The study did not involve wild animals.
Field-collected samples	The study did not involve samples collected from the field.
Ethics oversight	All mouse experiments were performed according to the guidelines of the animal ethics committee of WEHI

Note that full information on the approval of the study protocol must also be provided in the manuscript.

Human research participants

Policy information about studies involving human research participants

Population characteristics	Patient 1 Female 10 yrs Patient 2 Female 82 yrs Patient 3 Male 55 yrs Patient 4 Female 54 yrs Patient 5 Male 22 yrs Patient 6 Female 20 yrs. Patient 7 Male 13 yrs. All had Recurrent fevers. For more information please see Table 1.
Recruitment	Families were enrolled and evaluated in the Clinical Center at the National Institutes of Health under a protocol approved by the Institutional Review Board of the National Institute of Diabetes and Digestive and Kidney Diseases and the National Institute of Arthritis and Musculoskeletal and Skin Diseases. All subjects provided written informed consent. Patients with unexplained recurrent fevers were recruited.
Ethics oversight	All experiments in human samples were performed according to the guidelines of the human ethics committee of the NIH.

Note that full information on the approval of the study protocol must also be provided in the manuscript.